RSC Advances

REVIEW

View Article Online
View Journal | View Issue

Cite this: *RSC Adv.*, 2015, **5**, 14610

Recent developments in heterogeneous photocatalytic water treatment using visible light-responsive photocatalysts: a review

Shuying Dong,[a] Jinglan Feng,[a] Maohong Fan,[cd] Yunqing Pi,[a] Limin Hu,[a] Xiao Han,[a] Menglin Liu,[a] Jingyu Sun*[b] and Jianhui Sun*[a]

Visible light-responsive photocatalytic technology holds great potential in water treatment to enhance purification efficiency, as well as to augment water supply through the safe usage of unconventional water sources. This review summarizes the recent progress in the design and fabrication of visible light-responsive photocatalysts *via* various synthetic strategies, including the modification of traditional photocatalysts by doping, dye sensitization, or by forming a heterostructure, coupled with π-conjugated architecture, as well as the great efforts made within the exploration of novel visible light-responsive photocatalysts. Background information on the fundamentals of heterogeneous photocatalysis, the pathways of visible light-responsive photocatalysis, and the unique features of visible light-responsive photocatalysts are presented. The photocatalytic properties of the resulting visible light-responsive photocatalysts are also covered in relation to the water treatment, *i.e.*, regarding the photocatalytic degradation of organic compounds and inorganic pollutants, as well as photocatalytic disinfection. Finally, this review concludes with a summary and perspectives on the current challenges faced and new directions in this emerging area of research.

Received 3rd November 2014
Accepted 7th January 2015

DOI: 10.1039/c4ra13734e

www.rsc.org/advances

[a]*School of Environment, Henan Normal University, Key Laboratory for Yellow River and Huai River Water Environmental and Pollution Control, Ministry of Education, Henan Key Laboratory for Environmental Pollution Control, Xinxiang, Henan 453007, P. R. China. E-mail: sunjh@htu.cn; Tel: +86-373-3325971*

[b]*Center for Nanochemistry (CNC), College of Chemistry and Molecular Engineering, Peking University, Beijing 100871, P. R. China. E-mail: sunjy-cnc@pku.edu.cn; Tel: +86-10-62757157*

[c]*Department of Chemical and Petroleum Engineering, University of Wyoming, 1000 E University Avenue, Laramie, WY 82071, USA*

[d]*School of Civil and Environmental Engineering, Georgia Institute of Technology, Atlanta, Georgia 30332, USA*

Dr Shuying Dong received her PhD in Environmental Sciences in 2014 at the School of Environment, Henan Normal University, China, under the supervision of Dr Jianhui Sun. She has engaged in research in the field of photocatalysis for water treatment for more than seven years and has published 13 research papers in peer-reviewed journals in such an area. She is currently an assistant professor at the School of Environment, Henan Normal University. Her current research interests center on the rational synthesis and mechanism exploration of visible light-responsive photocatalysts for wastewater treatment.

Dr Maohong Fan is an SER Professor in Chemical and Petroleum Engineering at the University of Wyoming, USA. He has led and worked on many projects in the areas of chemical production, clean energy generation, and environmental protection, which have been supported by various domestic and international funding agencies, such as NSF, DOE and EPA in the USA, and industrial companies, such as Siemens and Caterpillar. He has published over 175 refereed books, book chapters, and papers in different chemical and environmental engineering, energy, and chemistry journals.

1. Introduction

With the rapid development of industrialization and urbanization, as well as huge population increases, the urgent demand for, but acute shortage of, clean water sources have attracted immense attention all over the world. This difference in clean water demand and availability is expected to continue to deteriorate with respect to growing contamination, owing to the overwhelming discharge of contaminants and pollutants into the natural water cycle. As far as the environment is concerned, the reuse and recycling of wastewater effluents is thus necessary to augment the limited fresh water supply and to offset more possible water resources in the long run.[1] During the past few decades, a variety of practical strategies have been implemented to develop viable wastewater treatment technologies.[2–6] For instance, conventionally, biological treatments were designed to effectively eliminate assorted types of contaminants from wastewater in the short term; however, these techniques also normally lead to the production of secondary pollution,[7] some of which even involves the presence of health-threatening bacteria and soluble refractory organic compounds that are hard to remove.[8] In this regard, developing nondestructive, green, and sustainable methodologies for water treatment is hence of great significance.

To date, photocatalysis has been considered as one of the most appealing options for wastewater treatment, due to its great potential and high efficiency by using sunlight to remove organic pollutants and harmful bacteria with the aid of a solid photocatalyst.[9,10] Here, it is well known that the photocatalytic efficiency is not only influenced by the nature of the employed photocatalysts, but is also affected by the irradiated light source. Generally, the catalyst can be photo-activated by a photon with energy equal to or higher than its band-gap energy (E_g). A stronger irradiation intensity would normally induce more efficient photolysis reactions.[11] As a safe and renewable energy source, natural sunlight is the ideal source to supply energy for these activation processes. Moreover, solar energy possesses special advantages, such as its cleanness and abundance. The sun delivers about four-orders of magnitude larger energy to the earth's surface per year than the energy annually used by humans all over the world.[12,13] To better utilize this solar energy to tackle water contamination issues, it is strongly desirable to explore novel catalysts with visible light-driven photocatalytic performance.

TiO_2 is the most widely studied photocatalyst, due to its cost-effectiveness, nontoxicity, and unique photocatalytic efficiency, as well as high stability. The basic mechanism of the photocatalytic degradation of pollutants using TiO_2 deals involves the absorption of near-UV light by TiO_2, the input of the light energy to induce charge separation to form electron (e^-)–hole (h^+) pairs, and the participation of e^- and h^+ in the oxidation–reduction reactions with suitable substrates.[14] However, there are a number of drawbacks of pure TiO_2 in photocatalysis, including the relatively large band-gap and the related fact that it can only absorb a small portion of UV radiation.[15] To facilitate the usage of energy from natural sunlight, certain routes have been attempted to modify TiO_2 accordingly, including non-/transition-metal ion doping,[16,17] sensitization,[18] ion implantation,[19] narrower band-gap semiconductor coupling,[20] and π-conjugated structure compositing,[21] *etc.* For example, Rey *et al.*[16] synthesized TiO_2–WO_3 photocatalysts, which exhibited higher catalytic activity than that of pure TiO_2 for the removal of a mixture of emerging contaminants through photocatalytic ozonation under visible light radiation. A study conducted by our group demonstrated that nitrogen-doped TiO_2 showed superior photocatalytic performance than that of the commercial Dugussa P25 TiO_2 for the degradation of a specific azo dye (Orange G) under visible light irradiation, which was attributed to the fact that nitrogen doping gave rise to the appearance of a new absorption band in the visible region.[17]

Dr Jingyu Sun received a BSc in Materials Sciences and Engineering from Zhejiang University, China in 2008, where he obtained the Honors degree from the Mixed Class, Chu Kochen Honors College. He obtained his DPhil in 2013 from the Department of Materials, University of Oxford, UK, for his work on the controlled growth of carbon nanomaterials on perovskite substrates. He is currently a postdoctoral associate in the Center for Nanochemistry, Peking University, where he works on graphene synthesis and related applications.

Dr Jianhui Sun (Professor, Henan Normal University, China) obtained his PhD in Environmental Sciences at the Guangzhou Institute of Geochemistry, Chinese Academy of Sciences, China. His water environment and pollution control research laboratory at the School of Environment, Henan Normal University is active in the field of photocatalysis, advanced oxidation technology, wastewater treatments and developing new approaches/concepts suitable for water and energy related applications. He has published over 50 research papers in peer-reviewed journals of international repute (h-index = 18). Dr Sun has teaching experience in Environmental Monitoring and Environmental Pollution Control.

There has been a growing interest lately in the development of directly visible light-responsive photocatalysts for water treatment, partially due to the complex and costly steps involved in the modification of the UV-illuminated ones.[22] To this end, a plethora of photocatalysts have been created, *e.g.*, SnS_2,[23] $CuO/BiVO_4$,[24] ZnS,[25] g-$C_3N_4/BiPO_4$,[26] $AgBr/Ag_3PO_4$/MWCNTs,[27] Ag_3PO_4,[28] BiOX (X = Cl, Br, I),[29] Bi_2MO_6 (M = W, Mo),[30,31] and MWO_4 (M^{2+} = Co, Cu, Pb, Cd, Mn and Zn),[32] $ZnSnO_3$,[33] MVO_4 (M = Bi, Sm),[34,35] nanostructured iron(III) oxides,[36] and oxynitride,[37] where considerable advances with regard to the photocatalytic performances have been steadily achieved, opening up the possibility for the practical usage of natural solar energy for wastewater degradation, as well as for environmental protection. For example, Mondal *et al.*[23] demonstrated that the dosage of variable concentrations of thioacetamide enabled the congregation of SnS_2 nanoflakes to nanoflowers and nanoyarns, which were proven to be promising for promoting the photoreduction of toxic Cr(VI) wastewater under visible light irradiation. Moreover, the performance of the SnS_2 nanoflower was found to be superior to that of the nanoyarn, owing to the increased surface area and higher pore volume. Sheng *et al.*[30] probed the photocatalytic activities of Bi_2WO_6 under visible light conditions using phenol degradation as a model reaction, where the observations obtained by employing spin-trapping electron paramagnetic resonance spectroscopy indicated that the irradiated Bi_2WO_6 was responsible not only for the production of $^{\bullet}OH$ radicals (*via* water oxidation), but also for the generation of H_2O_2 (*via* a two-electron reduction of O_2).

From a practical application point of view, solid-substrate-supported photocatalysts have in particular been recognized as an important class of industrial catalysts that are closely related with versatile key technologies in water treatment. These supported catalysts were found to possess several advantages, such as improved resistance to agglomeration, good accessibility of the substrate molecules, site isolation, practical usage in continuous-flow systems, and mechanical robustness, *etc.*[19,22,38–41] Moreover, such materials enabled the direct integration of technological devices to improve the photocatalysts' activity.[39] For example, Carraro *et al.*[40] prepared polymorphous iron(III) oxide nanosystems [α-Fe_2O_3 (hematite) and β-Fe_2O_3 (bixbyite)] *via* a chemical vapor deposition approach, which were well characterized and tested in the photo-degradation of methylene blue (MB) in the liquid phase under simulated solar light irradiation. The obtained results showed a significant dependence of the purity and morphology on the synthetic conditions, and where the surface area of the sample appeared to have a critical influence on the photocatalytic performance. Aziz *et al.*[41] fabricated a magnetically separable TiO_2 nanocomposite with SiO_2 coating (supported on a permanent magnet $NiFe_2O_4$), where the prepared TiO_2 material featured a lower band-gap energy (2.26 eV) and higher visible light absorption than that of pure TiO_2 (2.76 eV). Accordingly, the nanocomposite exhibited improved sunlight activity for the photodegradation of 2,4-dichlorophenol, as well as a good stability against the loss of its magnetic property for reuse.

This field of research has stimulated great efforts on the preparation, modification, and application of visible light-responsive photocatalysts, resulting in many important findings being reported during the past few years. Many insightful review articles have dealt with the target synthesis, theoretical investigation, photocatalysis design, and possible applications of photocatalysts, especially focusing on the specific modification of certain types of photocatalysts. In contrast, few reviews are concerned with the discussion of photocatalysis in the broader context of visible light-responsive photocatalyst types, *i.e.*, the routes to affording the visible light responses, the effects of the corresponding properties, and their related application within water treatment. Based on the aforementioned facts, the present review summarizes the latest developments in visible light-responsive photocatalysis, with a focus on the broad coverage of the employed catalyst systems. The review starts with a brief introduction to the fundamentals and speculated mechanisms of visible light-responsive photocatalysis, followed by a discussion of the recent achievements made in the design, modification, and applications of visible light-responsive photocatalyst systems. Finally, the future outlooks and perspectives are also considered.

2. Fundamentals and proposed pathways of visible light-responsive photocatalysis

In general, the system of heterogeneous photocatalysis using semiconductor materials consists of a light harvesting antenna and several active species to facilitate the pollutant degradation. The series of chain oxidative–reductive reactions that occur at the photon-activated surface has been broadly proposed as:

$$\text{Photocatalyst} + h\nu \rightarrow h^+ + e^- \quad (2.1)$$

$$h^+ + H_2O \rightarrow {}^{\bullet}OH + H^+ \quad (2.2)$$

$$h^+ + OH^- \rightarrow {}^{\bullet}OH \quad (2.3)$$

$$h^+ + \text{pollutant} \rightarrow (\text{pollutant})^+ \quad (2.4)$$

$$e^- + O_2 \rightarrow {}^{\bullet}O_2^- \quad (2.5)$$

$${}^{\bullet}O_2^- + H^+ \rightarrow {}^{\bullet}OOH \quad (2.6)$$

$$2{}^{\bullet}OOH \rightarrow O_2 + H_2O_2 \quad (2.7)$$

$$H_2O_2 + {}^{\bullet}O_2^- \rightarrow {}^{\bullet}OH + OH^- + O_2 \quad (2.8)$$

$$H_2O_2 + h\nu \rightarrow 2{}^{\bullet}OH \quad (2.9)$$

$$\text{Pollutant} + ({}^{\bullet}OH, h^+, {}^{\bullet}OOH \text{ or } O_2^-) \rightarrow \text{degradation product} \quad (2.10)$$

When the semiconductor is irradiated by an input light possessing an ultra-band-gap energy ($h\nu > E_g$), a valence band (VB) electron (e^-) is excited to the conduction band (CB), leaving behind a photogenerated hole (h^+) at the VB. Accordingly, the produced e^-/h^+ pairs are able to migrate to the surface of the semiconductor and participate in redox reactions. The

photocatalytic reaction usually involves three main active species: a hydroxyl radical ($^{\bullet}OH$), h^+, and a superoxide radical ($^{\bullet}O_2^-$), where $^{\bullet}OH$ is the primary oxidant in the photocatalytic degradation of the pollutant in the aqueous solution. The generation of $^{\bullet}OH$ radicals normally *via* two routes, (i) H_2O and OH^- in the water environment are readily oxidized by photogenerated h^+ to form $^{\bullet}OH$ radicals; (ii) O_2 presented in the aqueous solution is reduced by photogenerated e^- to form $^{\bullet}O_2^-$ radicals, followed by reacting with h^+ (forming $^{\bullet}OOH$ radicals) and then further decomposition to produce $^{\bullet}OH$ radicals. Moreover, the photogenerated h^+ is widely considered as an oxidant for directly degrading organic contaminates, the capacity of which depends on the catalyst type and oxidation conditions.[42] It is to be noted that the photo-induced e^- can easily recombine with h^+ after their generation in the absence of electron or hole scavengers. In this regard, the presence of specific scavengers is vital for suppressing the charge recombination rates and for enhancing the efficiency of photocatalysis.

To design a photocatalyst capable of utilizing safe and sustainable solar energy effectively, several critical requirements need to be satisfied. First, the semiconductor material should have a smaller band-gap to allow it to absorb solar energy across a broad range of spectrum. Simultaneously, the semiconductor should have a relatively positive enough valence band for the ample production of h^+ and $^{\bullet}OH$ radicals.[43] Second, the catalyst should possess a particular platform/system for the efficient charge separation and transportation.[44,45] Moreover, the semiconductor materials should have good photoelectrochemical stability in the electrochemical reactions.[46]

Generally, along with the electronic band structures, other features such as the material choice, morphological architecture, crystallinity, and surface properties should also be taken into consideration when building up an efficient and stable visible light-responsive photocatalytic system.[47,48] The choice of the semiconductor materials is particularly important, since it determines the level of the visible light response and, hence, the overall efficiency. The right morphological architecture with a short distance between the photocarrier-generating junction and the redox reaction center can effectively improve the carrier separation and transportation.[49] Moreover, a high degree of crystallinity with crystal defects would minimize the interface recombination, thereby enhancing the efficiencies of the photogenerated electrons and holes to participate in the desired reactions.[50] The surface area of the photocatalysts, which depends upon the porosity and geometrical shape of the materials, also exerts a crucial effect on the photocatalytic activity, owing to the fact that the adsorption of pollutants is a critical step.[51]

3. Overview of visible light-responsive photocatalysts

3.1. Modification routes towards augmenting the visible light response of photocatalysts

Compared to other photocatalysts for wastewater treatment, TiO_2 and ZnO have received considerable attention, due to their advanced photocatalytic performance under UV light irradiation.[52,53] The drawback of these semiconductors, however, lies in the fact that they are inactive under visible light irradiation, due to their large band-gap, which impedes their usage as solar energy harvesting photocatalysts. To overcome such a vital deficiency, certain modifications toward the semiconductors system have been attempted to enable their visible light responses with good efficiency.

3.1.1. Doping. Doping plays an indispensible role in modifying the properties of functional photocatalyst materials, with, in particular, non-metal doping being intensively investigated, ever since nitrogen-doped TiO_2 was initially reported by Asahi and colleagues.[54] The effect of doping on the properties of a photocatalyst is governed by several factors, such as the type and concentration of the dopant, the fabrication method, and the physicochemical properties of the catalyst. Previous studies have indicated that non-metal doping possesses great potential for realizing visible light-responsive photocatalytic activity, in this regard, a plethora of non-metals have been explored as dopants for modifying the electronic structure of UV-illuminated semiconductors.[55] In particular, non-metal doping at the atomic level could preserve the inherent surface properties of the photocatalyst, since the dopants exist in the form of isolated atoms rather than as clusters within the surface.[56] Furthermore, the special distribution of dopant states is generally located closely above the VB maximum, making the photo-generated holes on these states oxidative enough for subsequent photo-reactions.[57]

Nitrogen doping has been the most intensively studied amongst all the non-metal dopants. Wang *et al.*[58] prepared N-doped TiO_2 by the heat treatment of commercial P25-TiO_2 in a NH_3 gas flow, and the product was characterized by a series of techniques to investigate the origin of the visible light response of N-doped TiO_2. The results indicated that N-doped TiO_2 possessed triplet g value electron spin resonance signals ($g = 1.987$, 2.004, and 2.024) and visible light absorption in a wavelength range of 400–520 nm, which were attributed to the formation of single-electron-trapped oxygen vacancies (denoted as SETOVs) in a certain chemical environment. The visible light photocatalytic activity of N-doped TiO_2 was co-determined by the formation of SETOVs in the TiO_2 matrix and by the existence of doped-N on the surface. Similarly, one of our previous studies also reported that N-doped TiO_2 showed higher photocatalytic activity than that of commercial Dugussa P25 TiO_2 under visible light irradiation, which could be due to the presence of a TiO_2 anatase structure, and a new absorption band in the visible region caused by the nitrogen doping.[17]

Carbon doping has been explored with consideration of its low cost and its potential for band-gap narrowing, which can help to achieve significant improvements in visible light absorption capabilities.[59–62] Chen *et al.*[60] synthesized pure anatase C-doped TiO_2 by a low-pressure flat-flame metal organic chemical vapor condensation method by eliminating the nitrogen doping possibility. They demonstrated that visible light absorption was attributed to the carbon doping, but that the carbon did not incorporate into the TiO_2 crystal, and instead located on the surface. They also claimed that the C–C bond was

responsible for the light absorption. Dai and colleagues[61] prepared porous C-doped Bi_2O_3 with a high visible light-responsive photocatalytic activity *via* a simple calcination of bismuth nitrate pentahydrate in a glycol solution. It was shown that the carbon was incorporated into the lattice of Bi_2O_3, as the absorption edge of C-doped Bi_2O_3 had an obvious red shift with augmented absorption intensity in the region of 450–530 nm, which was responsible for the enhanced photocatalytic activity over the pure one. Samadi and coauthors[62] utilized an electrospinning technique to fabricate multi-walled carbon nanotubes (MWCNTs)-doped ZnO nanofibers with visible light-responsive photocatalytic activity. Their study revealed that Zn–O–C bonds were formed and the energy band-gap of the composite was 2.94 eV, which was lower than that of the pure ZnO nanofiber (3.11 eV). Accordingly, a 7-fold enhancement in the photocatalytic activity was observed because of the delayed electron–hole recombination exerted by the synergistic effect between the MWCNTs and ZnO. However, compared to the N-doped photocatalysts, C-doped ones are considered to be more difficult to synthesize and hence have not been widely employed to date.[63]

The modifications of photocatalyst with noble and other metals such as Pt, Au, Ag, Cu, V, Ni, and Sn have also enabled the extension of the spectral response of photocatalysts well into the visible region.[64] However, a few studies have claimed that several metallic species (especially transition metals) may act as recombination sites for the photo-induced charge carriers, thereby lowering the quantum efficiency.[65] For instance, Li *et al.*[65] fabricated hierarchical V-doped rutile TiO_2 nanofibers by a flame burning method, which showed a higher doping level of V into the TiO_2 crystal lattices than that prepared by calcination treatments. However, the photocatalytic activity of the synthesized V-doped rutile TiO_2 nanofibrous have not yet been obviously enhanced due to the V doping, but this could be attributed to the fact that the V dopants served as electron–hole recombination centers. Vijayan *et al.*[66] prepared visible light-activated Pt–TiO_2 nanotubes by a hydrothermal technique, where Pt doping affected the morphology of the TiO_2 nanotubes. Their study revealed that Pt nanoparticles were uniformly distributed on the nanotube surface and that the doping by Pt enhanced the visible light photoactivity of TiO_2 nanotubes for the photo-oxidation of acetaldehyde. Electron paramagnetic resonance spectra revealed that coordinated sites and oxygen deficiency were created on the surface of the TiO_2 nanotube after calcination in a hydrogen atmosphere, which further interacted with the Pt centers to alter the electronic, optical, and chemical behaviors of the TiO_2 nanotube. One of our recent studies reported the synthesis of Sn-doped ZnO photocatalysts with augmented sunlight photocatalytic activity through a microwave-assisted route. The microstructure, morphology, and optical properties of the ZnO were greatly changed by the Sn doping, contributing to an enhanced sunlight photocatalytic activity (*e.g.*, 13% higher decolorization rate and 29–52% greater mineralization efficiency than that of pure ZnO for the degradation of MB solution).[67]

Co-doping with two or more suitable heteroatoms (non-metal–non-metal, metal–non-metal, and metal–metal) can lead to substantial synergistic effects with respect to changing the band structures (including the CB and VB levels) of the systems to obtain the desired photocatalytic redox ability and selectivity, to enhance the visible light harvesting and charge mobility, or to modify the morphological characteristics. Moafi and colleagues[68] prepared La–Zr-doped ZnO nanocomposites using a modified sol–gel method. Their characterization indicated that La–Zr-doped ZnO exhibited a smaller particle size than that of pure ZnO, and had a red-shift feature in the absorption band. Interestingly, the co-doping with La and Zr gave rise to the band-gap narrowing, as well as to an enhancement of the photoactivity. Wu *et al.*[69] synthesized C–N co-doped TiO_2 hierarchical spheres *via* a direct chelating process with the aid of several types of amine agents, where it was found that the optimal C and N doping concentrations were produced by using trimethylamine, which effectively reduced the band-gap of TiO_2 to 2.85 eV without affecting its crystallization. Moreover, it exhibited an eightfold photocatalytic activity higher than that of commercial Degussa P25 powders for the decomposition of rhodamine B (RhB). Sun *et al.*[70] prepared N–TiO_2, Pt–TiO_2, N–Fe–TiO_2, N–Ni–TiO_2, N–Ag–TiO_2, and N–Pt–TiO_2 photocatalysts by acid-catalyzed sol–gel processes, and further evaluated the corresponding photocatalytic activities *via* the photodegradation of phenol solutions under simulated sunlight irradiation. It is worth noting that certain types of transition metals (Fe and Ni in this case) exerted a negative effect on N-metal co-doped TiO_2 photocatalysis, whilst noble metals (Ag and Pt) showed an augmentation in photocatalysis. In particular, N–Pt–TiO_2 exhibited a six times higher photocatalytic efficiency than that of Degussa P25 under simulated sunlight irradiation. The synergistic effect of N–Pt co-doping was ascribed to the multivalent states of Pt.

3.1.2. Dye sensitization. A simple and interesting strategy for achieving effective visible light harvesting is the photosensitization of wide-band-gap semiconductors by appropriate sensitizer molecules. Dye photosensitization has been reported to be one of the most promising ways to extend the photoresponse into the visible region, and to possessing certain advantages over direct photocatalysis.[71–75] The visible light induced photocatalytic mechanism of the dye-sensitized photocatalyst has been proposed as:[71]

$$\text{Dye (D)} + h\nu \rightarrow \text{dye* (D*)} \quad (3.1)$$

$$\text{Photocatalyst} + \text{D*} \rightarrow {}^{\bullet}\text{D}^{+} + \text{photocatalyst } (e^{-}) \quad (3.2)$$

$$\text{Photocatalyst } (e^{-}) + O_2 \rightarrow \text{photocatalyst} + {}^{\bullet}O_2^{-} \quad (3.3)$$

$$e^{-} + {}^{\bullet}\text{D}^{+} \rightarrow \text{D} \quad (3.4)$$

$${}^{\bullet}O_2^{-} + H^{+} \rightarrow {}^{\bullet}\text{OOH} \quad (3.5)$$

$$2{}^{\bullet}O_2^{-} + 2H^{+} \rightarrow {}^{\bullet}O_2 + H_2O_2 \quad (3.6)$$

$$H_2O_2 + {}^{\bullet}O_2^{-} \rightarrow {}^{\bullet}\text{OH} + OH^{-} + O_2 \quad (3.7)$$

$$\text{Pollutant} + ({}^{\bullet}\text{OH}, {}^{\bullet}\text{OOH or } O_2^{-}) \rightarrow \text{degradation product} \quad (3.8)$$

The dye can absorb visible light to reach an excited state, which, in general, has a lower redox potential than that of the corresponding ground state. When the redox potential is lower than the CB of the semiconductor, the cationic radicals and conduction band electron can be easily formed if an electron is injected into the conduction band from the excited state.[71,72] Li *et al.*[72] showed that the photo-responses of the squarylium dye (ISQ) sensitized TiO_2 nanoparticles were remarkably extended to the visible light region, and that their photocatalytic activity under visible light irradiation was significantly enhanced. In such a system, the ISQ dye on the sensitized surface of TiO_2 could be easily excited from the ground state (D) to the excited state (D*) with the aid of visible light. This excited state dye species could then be converted to a semi-oxidized radical cation ($^{\bullet}D^{+}$) by the injection of an electron into the CB of TiO_2, as the lowest unoccupied molecular orbital (LUMO) level of the ISQ dye matched well with the CB of TiO_2, thus benefiting the charge transfer. Radicals such as $^{\bullet}O_2^{-}$, $^{\bullet}OH$, and $^{\bullet}OOH$ were then produced *via* a series of protonation and reduction steps. Finally, the $^{\bullet}OH$ radicals reacted with the MB molecules to produce the degradation product.

Furthermore, the transportation of molecules adsorbed on the surfaces was reduced at a dimensional level, which is beneficial to the reaction kinetics and results in the extension of the excitation energy range of a semiconductor into the visible region. This may also possess the capability to drive other reactions, and hence the sensitivity of the photocatalytic process for the removal of colored pollutants can be increased in the presence of low concentrations of colored pollutants.[73] This approach is useful for treating textile wastewater, and one of the consequences of this is the direct oxidation of the dye. Shang *et al.*[74] demonstrated that the enhanced photocatalytic activity of dye-sensitized TiO_2 could be attributed to the wider absorption spectrum range and the electron transferred from the excited state of the dye molecule directly to the CB of TiO_2, which results in a greater number of electrons in the CB of TiO_2 and the consequent production of more active oxygen species. Li *et al.*[75] found that sensitized ZnO microrods with porphyrin hetero-aggregates have an enhanced visible light photocatalytic activity compared to those of porphyrin-monomers–modified ZnO and pure ZnO, which could be attributed to the redox potential of the porphyrin hetero-aggregate matching well with the energy level of ZnO and the consequent promotion of the electron injection from the excited state of porphyrin into the CB of ZnO, correspondingly suppressing the electron–hole recombination rates. Yang *et al.*[76] probed the usage of Alizarin Red S dye-sensitized nanoscale ZnO for the photocatalytic removal of Cr^{6+} from an aqueous solution under visible light irradiation. The apparent band-gap energy of the dye-sensitized nanoscale ZnO (2.79 eV) was narrower compared with that of nanoscale ZnO without dye sensitization (3.37 eV). It was suggested that the dye molecule, acting as an organic semiconductor, might exert an effect on the charge transition into the CB of ZnO in the excited state.

3.1.3. Heterostructure. Heterostructured semiconductors are another class of photocatalysts that utilize visible light for photocatalytic water treatment. When a wide-band-gap semiconductor is coupled with a narrow-band-gap semiconductor with a more negative CB level, enhanced electron–hole separation will be achieved, since the CB electrons can be injected from the narrow-band-gap semiconductor to the wide-band-gap semiconductor. Furthermore, the visible light response originates from the visible light photocatalytic activity of the narrow-band-gap semiconductor, as well from the synergistic effect in the heterostructure. The process is similar to dye sensitization, except for the following two differences: (1) electrons are injected from one semiconductor in to the other semiconductor, rather than the scenario of going from an excited dye to semiconductor; (2) the visible light harvesting antenna is from one semiconductor rather than from a dye. In this field, great efforts have been made in the synthesis of different coupled semiconductors, such as TiO_2/Bi_2WO_6,[77] ZnO/CdSe,[78] $Ag/Ag_3PO_4/TiO_2$,[79] CuS/ZnO,[80] CdS/TiO_2,[81] and $Bi_2O_2CO_3/Bi_2MoO_6$.[31] Compared to single-phase photocatalysts, such coupled systems usually possess enhanced visible light photocatalytic activity, due to the fact that the heterostructured combination extends the light-response range by coupling suitable electronic structures in materials and promoting the separation of photoexcited electron–hole pairs through various charge-transfer pathways. The heterostructure can compensate for the disadvantages of the individual components by inducing a synergistic effect, such as the improvement of photostability, as well as keeping the redox reactions separate at two different reaction sites. A three-dimensional (3D) TiO_2/Bi_2WO_6 hierarchical heterostructure was prepared for the photocatalytic decomposition of RhB in water under visible light irradiation. The improved photocatalytic performance could be ascribed to the improved light harvesting ability and an efficient separation of the photon-generated carriers.[77] Meanwhile, Wu *et al.*[78] confirmed that a ZnO/CdSe heterostructure exhibited improved visible light-responsive photocatalytic efficiency compared to that of pure ZnO, owing to the fact that the incorporation of CdSe could extend the absorption spectrum to the visible light region and suppress the recombination of photogenerated electron–hole pairs. Another example is the study performed by Lee *et al.*,[80] which revealed that a CuS/ZnO nanowire heterostructure exhibited superior photocatalytic activity and cycle performance under visible light compared with that of bare ZnO nanowire. The advanced photocatalytic activity was due to the interfacial charge transfer from the VB of the ZnO to that of the CuS, also reducing CuS to Cu_2S.

In addition to the extension of the light-response range and promotion of the separation of photon-generated carriers induced by the heterostructure nature, the photocatalytic performance of such a coupling system is crucially related to the size, shape, and surface area of the heterostructure. Wei *et al.*[81] dispersed CdS nanoparticles within the entire surface of the TiO_2 nanofibers, forming a CdS/TiO_2 hierarchical heterostructure. The enhanced photocatalytic activities of the CdS/TiO_2 heterostructure might have arisen from the increased surface area, extended light absorption region, and/or the favorable electron-transfer properties. Recently, Xu *et al.*[31] teamed up the wide-band-gap $Bi_2O_2CO_3$ with Bi_2MoO_6 to form hierarchical $Bi_2O_2CO_3/Bi_2MoO_6$ heterostructured

photocatalysts with superior visible light photocatalytic activity toward the degradation of RhB. The $Bi_2O_2CO_3/Bi_2MoO_6$ heterostructure also displayed visible light photocatalytic activity for the destruction of *E. coli*, with excellent stability and recycling performance. In this regard, the photocatalytic degradation efficiency was related to the Bi/Mo molar ratio, where the highest degradation efficiency was observed with a Bi/Mo molar ratio of 2.88/1, which was approx. 55% and 97% higher than that of the pure $Bi_2O_2CO_3$ microspheres and Bi_2MoO_6 nanoplatelets, respectively. Moreover, Zhou *et al.*[82] claimed that energy-band matching was responsible for the enhanced photocatalytic activity within the heterostructured systems from the results obtained by carrying out a comparison study between PdO/TiO_2 and Pd/TiO_2 heterostructured nanobelts.

3.1.4. Coupling with a π-conjugated structure. In recent years, the use of photocatalysts hybridized with a π-conjugated structure material has proven to be an effective route for enhancing visible light-responsive photocatalytic activity. Conventional photocatalysts, such as ZnO and TiO_2, unexceptionally presented superior visible light photocatalytic performances over those of the pristine materials after the proper hybridization with graphene,[83–85] C_{60},[86,87] C_3N_4,[88] polyaniline (PANI),[89,90] or polypyrrole (PPy).[91] These π-conjugated structure materials have shown great promise for modifying wide-band-gap inorganic semiconductors in the fabrication of visible light-responsive photocatalysts, mainly due to the presence of their π-conjugated electron systems, high mobility charge carriers, high absorption coefficients in the visible part of the spectrum, and good environmental stability. Moreover, many conjugated structure materials have also been identified as efficient photo-generated e^- transporters upon visible light excitation. In photocatalysis, graphene (along with graphene oxide and reduced graphene oxide (RGO)) has been proven to be an ideal support for constructing photocatalytic composites. When graphene was introduced to hybridize with TiO_2, it could simultaneously improve the light absorption, narrow the band-gap, and suppress the recombination of photo-generated electron–hole pairs.[83] Meanwhile, Thomas *et al.*[84] decorated carboxyl functionalized few-layer graphene with TiO_2, and the obtained composites showed a remarkable improvement in visible light-driven photocatalysis. The enhanced visible light photocatalytic activity was attributed not only to their improved electron hole mobility, but also to their enhanced surface adsorption ability for molecules through π–π interactions. Min *et al.*[92] demonstrated that the usage of different routes to chemically anchoring TiO_2 nanoparticles onto graphene by chemical interactions, such as chemisorption, electronegativity, and coordination, could lead to a great enhancement of their photocatalytic activity under visible light, due to the full and intimate contact through chemical bonds of Ti–C and Ti–O–C, but that there was no such enhancement under UV-light. Gayathri *et al.*[93] showed that the formation of ZnO/graphene composites promoted absorption in the visible region and enhanced visible light photocatalytic activity compared with the pristine ZnO. Very recently, our group[94] decorated ZnO nanoclusters with prepared RGO to form novel ZnO/RGO nanocomposites, and found that the photocatalytic activity in the visible light-driven degradation of metronidazole with the ZnO nanoclusters could be enhanced by coupling with RGO, attaining an approx. 32.4% increase compared with that of pure ZnO (see Fig. 1).

C_{60} possessing a unique configuration and properties has been widely studied. C_{60} has a closed-shell configuration consisting of 30 bonding molecular orbitals with 60 π-electrons, which could efficiently cause a rapid photogenerated charge separation and a relatively slow charge recombination.[95] Fu *et al.*[86] found that C_{60}-hybridized ZnO showed the same absorbance edge as pure ZnO, but an extended absorbance to the visible region. The photocorrosion inhibition of ZnO by coupling with C_{60} could be attributed to the reduced activation of the surface oxygen atom. Due to the interaction of C_{60} and ZnO with the aid of a conjugative π-system, a higher migration efficiency of photogenerated electrons could be produced at the interface of C_{60} and ZnO, which can bring about a greater photocatalytic activity for C_{60}-hybridized ZnO. Long *et al.*[87] reported that the photocatalytic activity of C_{60}-incorporated TiO_2 nanorods under visible light irradiation was dramatically increased by a factor of approximately 3.3 and 2.7 when compared with that of pure TiO_2 nanorods and Degussa P25, respectively, which was ascribed to the effective separation of the photogenerated carriers with the introduction of C_{60}.

As one of the π-conjugated structure materials, graphite-like carbon nitride (g-C_3N_4) has recently been investigated to see if it exhibited good photocatalytic activity for wastewater treatment under visible light irradiation.[96,97] In comparison with the aforementioned π-conjugated structure, g-C_3N_4 is a soft polymer, so it should be easy to decorate on the surface of a photocatalyst, promoting the formation of core–shell structures. Sun *et al.*[96] synthesized g-C_3N_4–ZnO composite photocatalysts with different ZnO dosages in wt% by a simple calcination process, the absorption edge of which shifted toward the lower energy region and longer wavelengths in comparison with that of pure ZnO and g-C_3N_4. The remarkable photocatalytic activity of the g-C_3N_4–ZnO composite for the photodegradation of methyl orange and *p*-nitrophenol under visible light irradiation could be mainly ascribed to the enhancement of the electron–hole separations at the interface of ZnO and g-C_3N_4. Fu *et al.*[97] prepared g-C_3N_4–TiO_2 composite samples with different weight ratios by heating mixtures of melamine and commercial TiO_2. The samples with weight ratios of g-C_3N_4 : $TiO_2 = 2.5$ exhibited the highest adsorption capacity and enhanced visible light catalytic activity for the degradation of methylene blue. The excited electrons on the surface of g-C_3N_4 could transfer easily to the TiO_2 CB *via* the well-built heterojunction, correspondingly inhibiting recombination of the photogenerated electron–hole pairs.

Conjugated polymer modification is one of the most promising methods for modifying TiO_2 to prepare visible light-responsive photocatalysts. In the combined system of a conjugated polymer and a semiconductor, it is thermodynamically possible to transfer the electrons from the conjugated polymer to the TiO_2 CB under visible light irradiation, due to the fact that the conjugated polymer LUMO is energetically higher than the TiO_2 CB edge. Therefore, the occurrence of interfacial charge

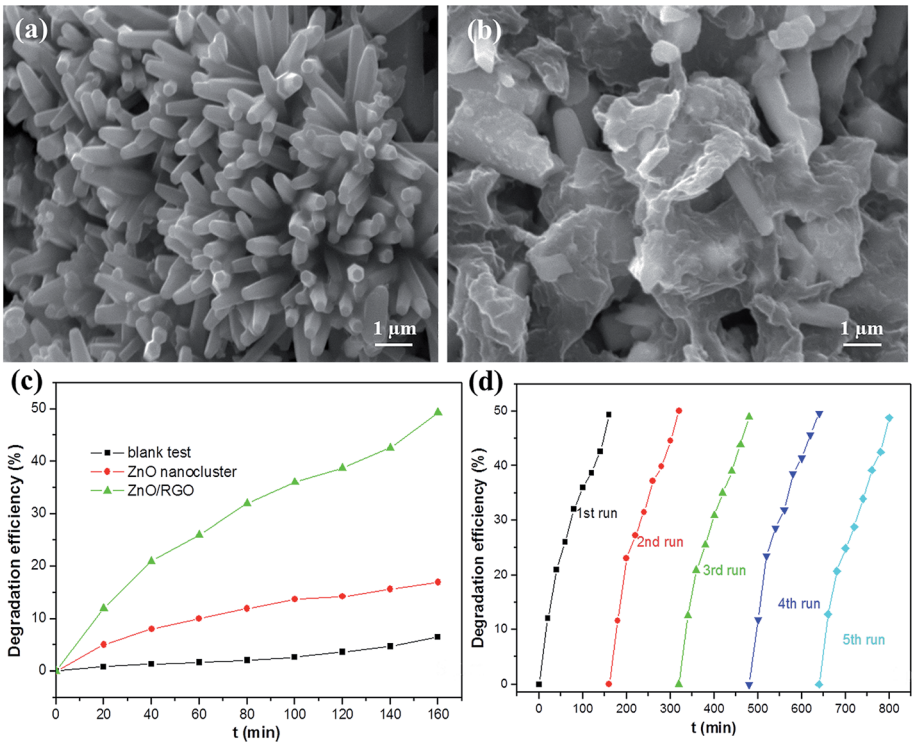

Fig. 1 SEM images of the as-synthesized ZnO nanoclusters (a) and ZnO/RGO nanocomposites (b). (c) The degradation efficiencies of metronidazole-contained wastewater using the ZnO nanoclusters and ZnO/RGO nanocomposites under visible light irradiation. (d) Cycling runs of the ZnO/RGO nanocomposites for the photo-degradation of metronidazole. Reproduced with permission from ref. 94.

transfer and separation between the conjugated polymer and the semiconductor guarantees an advanced photoresponse to visible light.[89] Li *et al.*[90] prepared a PANI-modified TiO_2 material using an *in situ* chemical oxidative polymerization method, where the enhanced visible light photocatalytic activity, in terms of the phenol degradation, was due to the synergetic effect between PANI and TiO_2. Meanwhile, Deng *et al.*[91] and Luo *et al.*[98] observed a similar trend with regard to the enhancement of photocatalytic performances compared to the bare TiO_2 photocatalyst when probing the PPy-PANI-TiO_2^- and polyisoprene-modified TiO_2 systems, respectively.

3.1.5. Other modification techniques. Montmorillonite has also been employed to extend the light absorption region of photocatalysts, taking advantage of its several useful characteristics, such as high crystallization, strong cation exchange capacity, large specific surface area, and considerable number of active surface sites. For example, Li *et al.*[99] chose mesoporous montmorillonite as the supporting material for Sn^{2+}-doped TiO_2, where the absorption edges of the supported Sn^{2+}-doped TiO_2 displayed a red shift, and, consequently, exhibited higher visible light catalytic activity than that of unloaded Sn^{2+}-doped TiO_2. Zheng *et al.*[100] demonstrated that anatase TiO_2 films with dominant[101] facets exhibited higher RhB degradation efficiency. Moreover, defect-induced visible light-responsive photocatalysts can also be formed by introducing color centers within the material.[102] To date, hydrogenation has been demonstrated as an effective route to induce defects in the surface layers of nanophase TiO_2. The disorder-engineered TiO_2 nanocrystals exhibited good solar-driven photocatalytic activities, due to the marked extension of the optical absorption to the infrared range.[103] Another excellent candidate for the modification of photocatalysts is the integration of wide-band-gap semiconductors with plasmonic metal nanocrystals, which benefit from the increased concentration of photogenerated carriers and from efficient utilization of visible light *via* plasmon-enhanced light absorption.[104]

3.2. Novel visible light-responsive photocatalysts

3.2.1. Multi-component oxides. Multi-component oxides, as a new type of narrow-band-gap photocatalysts with complex constitutions, have recently received extensive attention in the field of photocatalysis. Bismuth-based multi-component oxides have been heavy investigated because of their great visible light-responsive photocatalytic activity, which has been proven to be superior to that of traditional TiO_2.[105] The narrow band-gap of bismuth-based multi-component oxides originates from the valence band consisting of Bi_{6s} and O_{2p} orbitals, which are more negative than those consisting of only O_{2p} ones (TiO_2).[106] Our recent studies on $BiVO_4$ indeed revealed that $BiVO_4$ exhibited excellent visible light or natural sunlight photocatalytic activity.[107–110] In particular, the photocatalytic performances of $BiVO_4$ strongly rely on the shape configurations (as shown in Fig. 2). Concerning other bismuth-based multi-component oxides, Dai *et al.*[111] demonstrated that Bi_2WO_6 hierarchical hollow spheres with an ultrahigh specific surface area possessed superior visible light photocatalytic activity for the

degradation of RhB over other morphological products. Very recently, Shang *et al.*[112] reported that $Bi_{24}O_{31}Br_{10}$ presented higher activity than that of Bi_2O_3 and BiOBr for the photocatalytic reduction of Cr(VI) ions under visible light irradiation. Moreover, bismuth titanate ($Bi_{12}TiO_{20}$) nanostructures with different morphologies have also been synthesized, exhibiting advanced photocatalytic activity over traditional N-doped TiO_2 in terms of the degradation of acid orange 7.[51]

The photocatalytic properties of other multi-component oxides towards the degradation of organic contaminants under visible light irradiation have been investigated. In one study, Ag_3PO_4 nanoparticles were synthesized by an ion-exchange reaction and nearly 80% of Cr(VI) ions were removed after visible light irradiation in Ag_3PO_4 suspension, where the excellent photocatalytic reduction performance was attributed to the high separation efficiency of the photogenerated charges.[28] Another study was concerned with the synthesis of $CaIn_2O_4$ rods, as well as measurements of MB degradation and toluene oxidation under visible light irradiation.[113] In particular, MIn_2O_4 (M = Ca, Sr, and Ba) semiconductors were employed for the degradation of MB under visible light irradiation, where the highest photocatalytic activity was obtained using $CaIn_2O_4$.[114]

3.2.2. Nanocomposites. There has been considerable effort made to seek novel photocatalysts that are capable of harvesting visible light. Amongst the semiconductors with potentially good photocatalytic activities, considerable attention has been given to nanocomposites with tunable band-gaps, which offer an opportunity to extend the absorption wavelength from the UV to the visible light region. Moreover, compared with a single phase semiconductor, composites could promote the generation and separation of photogenerated carriers, and hence could dramatically enhance the photocatalytic activity. The intercalation of bismuth-based oxides, $ZnSnO_3$, $SmVO_4$, CeO_2, Bi_2MoO_6, $Fe_{0.01}Ni_{0.01}Zn_{0.98}O$, and $ZnFe_2O_4$ particles into mesoporous materials, such as graphene, g-C_3N_4, C_{60}, PANI, and multi-walled carbon nanotubes (MWCNTs), has been reported,[33,35,115–121] where intercalation extends the absorption spectrum region. When these intercalated nanoparticles are excited by a band-gap irradiation, the photo-generated electrons and holes can be more efficiently utilized, due to the high surface area to bulk ratio of the mesoporous structure. In the $BiVO_4$/RGO composites, the photo-generated e^- by sunlight irradiation in the CB of the $BiVO_4$ could be injected into RGO, while photo-generated holes remained in the VB of the $BiVO_4$, thereby directly oxidizing the RhB molecules adsorbed on the surface of $BiVO_4$. This charge-carrier separation was responsible for the improved photocatalytic activity.[115,116] In our case, we prepared novel $ZnSnO_3$ hollow nanospheres on reduced graphene oxide (RGO), and the as-prepared hybrid nanocomposites exhibited excellent photocatalytic activities for the decomposition of metronidazole under visible light irradiation (see Fig. 3). The

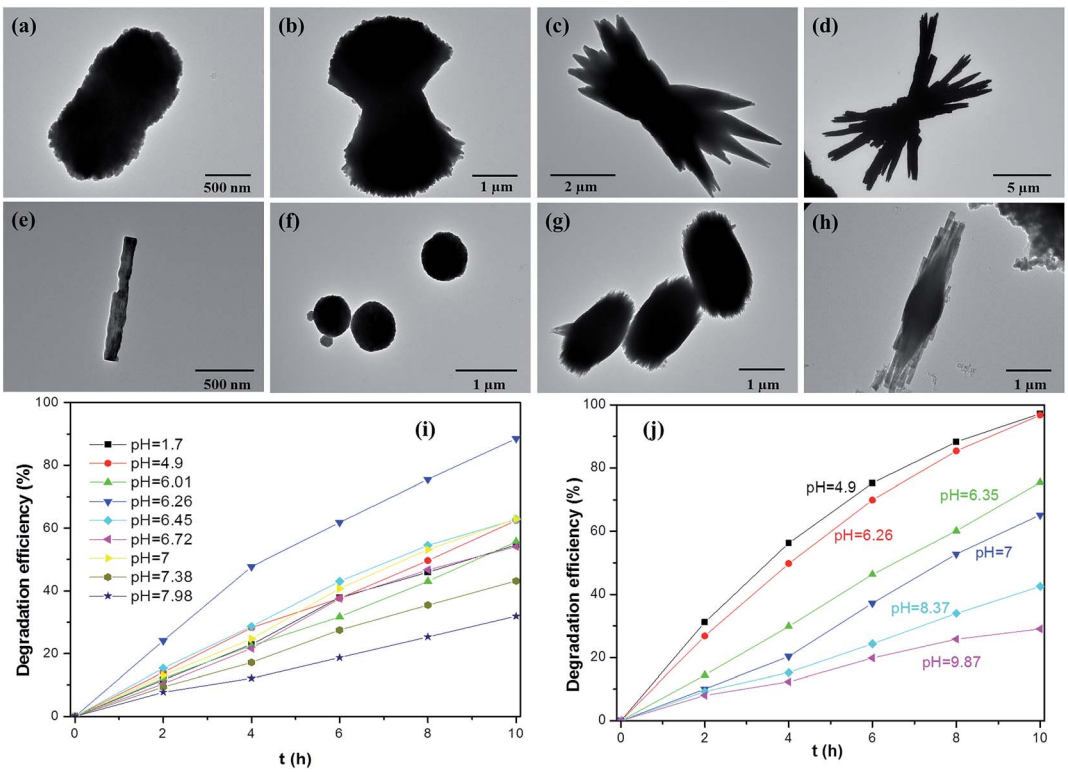

Fig. 2 Representative TEM micrographs of different-shaped $BiVO_4$ hierarchical structures obtained by varying the pH values of the precursors using $NH_3 \cdot H_2O$ (a) pH = 4.9; (b) pH = 6.26; (c) pH = 6.72; (d) pH = 7; (e) pH = 7.3; and NaOH (f) pH = 4.9; (g) pH = 6.26; (h) pH = 7 as the pH controlling agent. The photocatalytic degradation of RhB under natural sunlight irradiation over (i) A-$BiVO_4$ and (j) S-$BiVO_4$ samples prepared at different pH values of the precursors. Reproduced with permission from ref. 107.

enhanced photocatalytic activity was due to the advanced adsorption efficiency of the molecules, the reduction in the electron–hole recombination rate, and the enhanced visible light absorption within the hybrid nanocomposites due to the introduction of RGO.[33]

The novel g-C_3N_4/$SmVO_4$ composite photocatalyst with improved visible light photocatalytic activities for RhB degradation was investigated by Li and colleagues.[35] The improvement originated from the synergetic effect of g-C_3N_4 and $SmVO_4$ based on the band position; the schematic illustration of the electron–hole separation and transport at the visible light-driven g-C_3N_4/$SmVO_4$ composite photocatalyst is shown in Fig. 4. Channei *et al.*[117] showed that Fe_3O_4/SiO_2/CeO_2 core–shell magnetic structures had a higher photocatalytic degradation rate for formic and oxalic acid than that of bare CeO_2 under visible light. Zhang *et al.*[118] reported the formation of Bi_2O_3/Bi_2SiO_5 nanoheterostructures within mesoporous SiO_2 microspheres, which exhibited excellent photocatalytic activities for the degradation of both acetaldehyde and bisphenol A under simulated solar light irradiation. The high photocatalytic efficiency was due to the efficiency charges separation, stemming from the heterostructure junction effect. The C_{60}-modified Bi_2MoO_6 photocatalyst showed high photocatalytic activity in the reduction of bromate ions under visible light irradiation.[119] The enhanced photocatalytic activity may be closely attributed to the interaction between Bi_2MoO_6 and C_{60}, which increases the photo-generated electron mobility in Bi_2MoO_6, and as such, C_{60} could effectively transfer the photoelectrons from the CB of Bi_2MoO_6 after being illuminated under visible light irradiation. Kant *et al.*[120] synthesized a $Fe_{0.01}Ni_{0.01}Zn_{0.98}O$/PANI composite by an *in situ* free radical polymerization method. Optical and photocatalytic studies revealed that the formation of the composite further enhanced the visible light absorption and photodegradation efficiency against MB under visible light irradiation. MWCNTs have the potential for use in the fabrication of novel nanocomposites, due to their special aperture structure, high aspect ratio, and large electron storage capacity. $ZnFe_2O_4$/MWCNTs composite has been found to be a suitable visible light-responsive catalyst for the degradation of RhB.[121] High-quality CuSe/ZnSe flower-like nanocomposites were fabricated as a visible light-responsive photocatalyst through utilizing the p–n junction effect and band-gap engineering. The 8 wt% CuSe/ZnSe sample exhibited over 4 times and 2.5 times degradation ratios for both MO and MB over that of the pure ZnSe sample, respectively. The improvements were attributed to the effective separation of the photogenerated carriers by the direct initiated interfacial charge transfer from the VB of ZnSe to CuSe, resulting in the reduction of CuSe to Cu_2Se.[122]

3.2.3. Other emerging visible light-responsive photocatalysts. ZrO_2/Dy_2O_3 materials with tunable compositions have been synthesized and have exhibited good photocatalytic degradation performances over both RhB and MB under visible light irradiation, which result from their special defect structure, small crystal size, and large specific surface area.[123] $Bi_2Mo_xW_{1-x}$ (x = 0–1) solid solutions have exhibited high photocatalytic activity for the degradation of RhB under visible light, which was mainly attributed to the special structure of the solid solution and the lower energy band-gap.[124] The catalytic

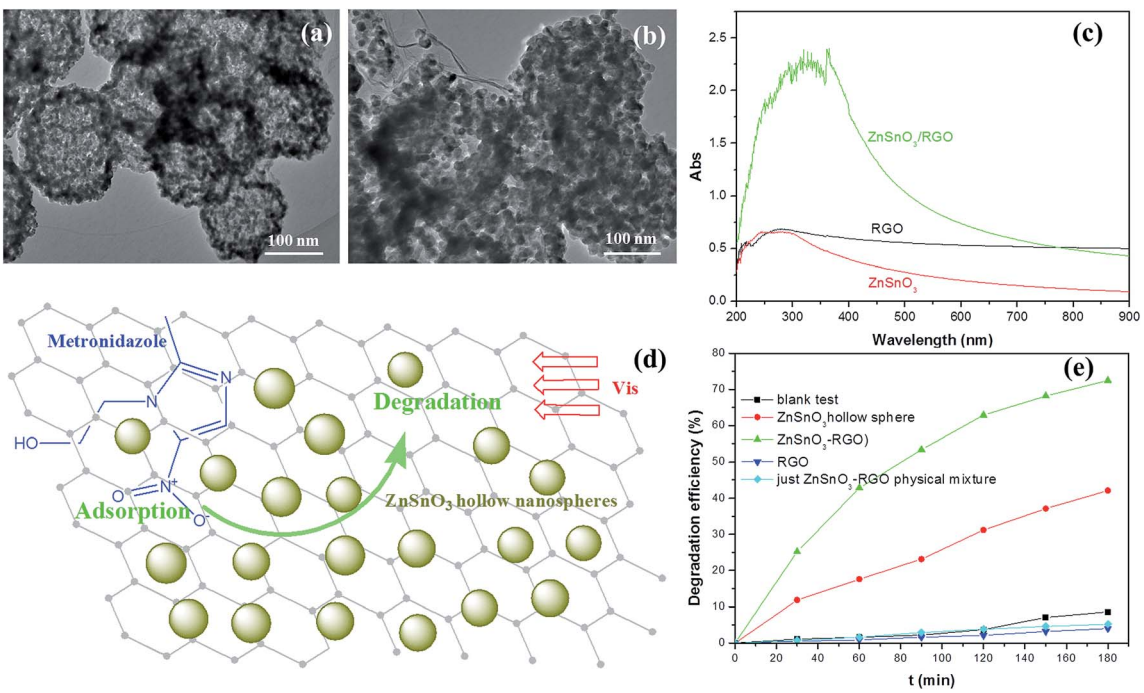

Fig. 3 The HRTEM images of the prepared $ZnSnO_3$ hollow nanosphere (a) and $ZnSnO_3$/RGO nanocomposite (b). (c) The UV-Vis absorption spectra of the RGO, pure $ZnSnO_3$ hollow nanosphere and $ZnSnO_3$/RGO nanocomposite. The speculated illustration (d) and degradation efficiencies (e) of the metronidazole wastewater by $ZnSnO_3$ hollow nanosphere and $ZnSnO_3$/RGO nanocomposite photocatalysts under visible light irradiation. Reproduced with permission from ref. 33.

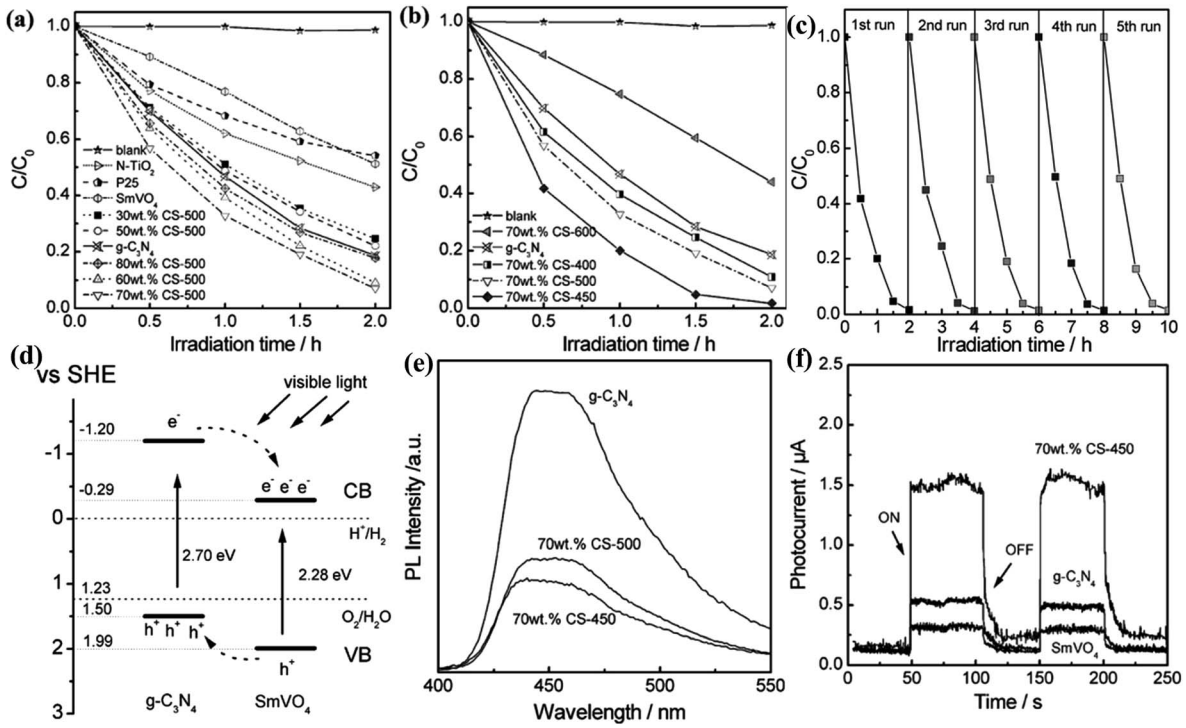

Fig. 4 Visible light-driven photocatalytic activity of g-C_3N_4/$SmVO_4$ composites with different g-C_3N_4 concentration (a) and 70 wt% g-C_3N_4/$SmVO_4$ calcined at different temperatures (b). (c) Cycling runs for the photocatalytic degradation of RhB in the presence of 70 wt% CS-450 sample under visible light irradiation. (d) A schematic for electron–hole separation and transport at the visible light-driven g-C_3N_4/$SmVO_4$ composite photocatalyst interface. (e) The photoluminescence spectra of pure g-C_3N_4 and g-C_3N_4/$SmVO_4$ composite. (f) Transient photocurrent response for $SmVO_4$, g-C_3N_4 and 70 wt% CS-450 samples. Reproduced with permission from ref. 35.

chemistry of polyoxometalates in promoting environmentally friendly photocatalytic process has also attracted considerable attention; examples include the novel $Ba_4(SiW^{V}_4W^{VI}_8O_{40})\cdot H_2O$ (ref. 125) and Bi^{3+}-doped $NaTaO_3$ powdered material.[126] Moreover, it has been shown that immobilizing palladium phthalocyaninesulfonate (PdPcS) integrated onto the FDU-15 mesopolymer provided a number of diamino groups inside the mesopores, which could be advantageous for excellent visible light photocatalytic activity and reusability.[127]

3.3. Unique features of visible light-responsive photocatalysts

A photocatalysis process can be defined as a photo-induced reaction on the basis of semiconductor materials, which involves transforming light into other forms of energy. In a visible light-responsive photocatalytic system, three key features should be considered. The first is the electronic structure, which determines the optical properties and band structure of the photocatalysts. The semiconductor should have the ability to absorb visible light and the band-gap needs to be narrow enough to be excited by visible light photons. The second key feature is the crystallinity; high crystallinity means less crystalline defects, which would be beneficial for lowering the e^{-}–h^{+} recombination rate. The final key feature is the surface character, which usually exerts a critical effect on surface chemical reactions such as oxidation by photo-generated holes and reduction by photo-generated electrons. The use of visible light-responsive photocatalysts to introduce suitable physicochemical properties is extremely common.

3.3.1. Optical properties and band structure. The optical property of photocatalysts is one of the crucial factors for predicting their photocatalytic performance. The UV-vis spectrum can elucidate that the outer electrons of atoms absorb radiant energy and undergo transitions to higher energy levels, exhibiting special features in the spectrum in the absorption region. Light irradiation provides the photons required for the electron transfer from the valence band to the conduction band of the photocatalyst.[128] Both light intensity and wavelength are important, due to the fact that (i) the overall energy input to a photocatalytic process relies upon the light intensity, and (ii) the energy of a photon is related to the light's wavelength. In addition, if a highly concentrated pollutant solution is used, the chance for direct light absorption by the catalyst is low, therefore giving rise to retarded catalytic activity. Soltani *et al.*[129] managed to extend the light absorption of ZnS and CdS nanoparticles to the visible region, where the stability of such materials against photo-corrosion, as well as against the degradation efficiency of dyes were improved. Tan *et al.*[130] demonstrated that Sm was partially introduced in the crystal lattice of $ZnIn_2S_4$ microspheres to produce a doping energy level, which then promoted the separation of photo-induced electron–hole pairs and enhanced the absorption of visible light, leading to a higher photodegradation efficiency of RhB under visible light irradiation.

Herein, another important point is that photo-absorption and e^-–h^+ generation are inextricably linked. Since the ability of a photocatalyst is exclusively governed by its band structure, from a thermodynamic point of view, estimation of the potential of the VB top and CB bottom is essential to predict the possibility of driving a photocatalytic reaction. A general way to carry out such estimation involves taking measurements of the optical absorption property, where the optical band-gap can be estimated using the following equation:

$$Ah\nu = C(h\nu - E_g)^n \quad (3.9)$$

where C denotes a constant, A, E_g, h, and ν represent the absorption coefficient, the band-gap energy, the Planck constant, and the incident light frequency, respectively. The band-gap energy (E_g) of the photocatalysts can be estimated from a plot depicting $(Ah\nu)^{1/n}$ *versus* $h\nu$. The constant n is 1/2, 3/2, 2, or 3 for a direct transition, forbidden direct transition, indirect transition, or forbidden indirect transition, respectively, where the forbidden direct or indirect transition is always neglected. Moreover, feasible e^- and/or h^+ transfer from one component unit to another with the proper band edge positions can greatly suppress the e^-–h^+ recombination probability and increase the lifetime of the charge carriers, thus promoting the photocatalytic efficiency. In this regard, Kanhere *et al.*[126] reported that the optical properties obtained by the band structure calculations were in good agreement with the experimentally observed absorption spectra.

The photocatalytic removal efficiency of MO, RhB, and MB was enhanced under both simulated solar light and visible light irradiation when the photonic band-gaps of the TiO_2 photonic crystals were well matched with the absorption peaks of the corresponding dyes. The improvement could be attributed to the intensified dye sensitization as a result of a slow photon effect on the edges of the photonic band-gaps.[131] When commercial TiO_2 crystals were coupled with a trace amount of narrow-band-gap Ag_2CO_3, the photocatalytic degradation activity under visible light irradiation of the composite was enhanced, due to the promoted visible light absorption and the suppressed recombination rate of the e^-/h^+ pairs.[132] It was also demonstrated that the optical properties of the Cu_2PO_4OH hierarchical superstructures were strongly related to their morphologies and the size of the assembled crystallites, where the walnut-shaped morphology exhibited the best photocatalytic performance, due to its excellent visible light absorption ability, as well as high BET surface area.[133]

3.3.2. Crystallinity. Photocatalysts are usually inorganic solid materials that are often crystals. The crystallinity often bonds together other features, such as optical properties, electronic structures, and photocatalytic performance. It is well known that $BiVO_4$ can exist in three crystalline phases, namely, zircon tetragonal (zt-$BiVO_4$), scheelite tetragonal (st-$BiVO_4$), and monoclinic clinobisvanite (m-$BiVO_4$). Ding *et al.*[134] investigated the electronic structures and optical properties of the three crystalline phases of $BiVO_4$ by DFT calculations. The results showed that zt-$BiVO_4$ was a semiconductor with a direct minimum band-gap, which was obviously larger than that of the indirect band-gap semiconductors st-$BiVO_4$ and m-$BiVO_4$. The zircon tetragonal phase also exhibited the most powerful oxidation and reduction ability, but the weakest visible light absorption ability, whilst the other two phases showed similar band edge positions and absorption spectra. zt-$BiVO_4$ exhibited distinct electronic properties due to having the shortest Bi–O bond, resulting in the strongest covalent interaction between Bi and O; whilst for the electronic structures, the distributions of the density of states, the atomic populations, and the atomic charges of st-$BiVO_4$ and m-$BiVO_4$ were quite similar. It is worth noting that m-$BiVO_4$ had the most dominant photocatalytic activity compared with the other crystalline phases, due to its excellent performance in the generation and separation of photoinduced carriers. TiO_2 has three crystalline polymorphs in nature: brookite, rutile, and anatase, where TiO_6 octahedrals with some extent of distortion are connected by shared corners and/or edges determining the crystal structure. Among these, anatase TiO_2 usually shows greatly superior photoactivity compared to rutile and brookite. The packing density discrepancy between anatase and rutile/brookite affects the bulk diffusion capability of carriers, which is another important factor in controlling the photoactivity, in addition to the stronger adsorptive affinity of anatase for organic molecules.[44] The mixtures of anatase/rutile, brookite/rutile, and anatase/brookite (anatase/rutile in particular) result in synergistic photocatalytic effects on charge-carrier transfer by forming an intimate contact in the interface of the two phases. Moreover, some dopants can exist as their oxide clusters instead of atoms within the surface/subsurface of doped matrices, due to the differences in crystal structure and crystal nucleation ability between the dopants and matrices. In addition, the doping-induced phase transformations of photocatalysts are also sensitive to how pristine the photocatalysts' crystal structures are.[135]

3.3.3. Surface features. One of the representative cases for studying the kinetics of reactions occurring on the photocatalyst surface is the so-called surface reaction limited process. Under this condition, surface adsorption is kept in equilibrium during the reaction, with the overall rate coinciding with the rate of reaction occurring on the surface. Therefore, in addition to the basic requirements of the electronic structure for the semiconductor in the photocatalytic systems, a favorable interface structure is also vital in promoting the interface transfer of carriers *via* different pathways. As is well-known, the adsorption ability of a photocatalyst is one of the essential factors influencing the photo-activity, because it is beneficial for the transfer of charge carriers between the radical ions of a pollutant and semiconductor. It has been demonstrated that the photocatalytic degradation efficiency relies greatly on the adsorption behavior between the target pollutant molecules and the photocatalyst, and that adsorption of the pollutant molecules on the catalyst can significantly improve the degradation efficiency.[136] It is of great importance then to investigate the adsorption process of pollutants on the photocatalyst surface, in order to clarify the mechanism of the photocatalytic reactions, which in turn, could facilitate their application in water purification. The surface of photocatalysts are positively

charged in acidic solutions and negatively charged in alkaline solutions.[129] Therefore, photocatalysts with different surface charges should exhibit a highly selective adsorption of charged targeted pollutants and a molecular recognitive photocatalytic performance *via* electrostatic attraction or repulsion.[137] The adsorption ability is also affected by the predominant atomic state for the electronegativity of the exposed facets.[130] For example, Tan *et al.*[130] found that hexagonal $ZnIn_2S_4$ with dominant {0001} facets exhibited a high adsorption ability toward cationic RhB, but only a weak adsorption ability toward anionic MO dye molecules, implying that the exposed {0001} facets of hexagonal $ZnIn_2S_4$ microspheres were beneficial for adsorbing cationic dye molecules. Further studies indicated that the surface electronegativity of the prepared $ZnIn_2S_4$ was the primary factor for the higher adsorption of RhB, and that the exposed S atom of the {0001} facets was the primary factor for the improved photocatalytic efficiency of hexagonal $ZnIn_2S_4$.

The redox potential of the reaction substrates, which adsorb on the surface depending on the amount of adsorbed substrates and on the surface chemical structure, depends more directly on the specific surface area. Table 1 summarizes the various preparation methods for visible light-responsive photocatalysts with various Brunauer–Emmett–Teller (BET) surface areas. In general, a high surface area to volume ratio of photocatalysts appears to be an important parameter for designing and engineering photocatalytic materials. For example, Dai *et al.*[61] prepared C-doped Bi_2O_3 with a porous structure by a simply calcination of $Bi(NO_3)_3 \cdot 5H_2O$ in glycol solution. The porous materials possess a larger specific surface area, which then contributed to more possible reaction sites on the photocatalyst surface, as well as facilitating the rapid diffusion of ions and molecules within the material, resulting in a higher photocatalytic activity. Kim *et al.*[138] reported that the dye degradation performance was further markedly enhanced under visible light irradiation with a dramatic increase in the BET surface area, with an order of 2D BiOCl ($5.5\ m^2\ g^{-1}$) < 3D BiOCl ($16.8\ m^2\ g^{-1}$) $\ll$ $BiOCl_{0.6}I_{0.4}$ ($46.6\ m^2\ g^{-1}$). Such investigations indicate that the specific surface area plays an important role in the photodegradation of pollutants. Moreover, the photocatalytic performances are not solely related to the surface area, but are also influenced by the surface charge, crystal facets, band structure, and optical properties, *etc.* For instance, owing to the change of surface charge and the newly created recombination center with Ag-loading, the photocatalytic degradation performance of Ag-doped $BiOCl_{0.6}I_{0.4}$ was dramatically reduced upon loading with small amounts of Ag, although the BET surface area increased from $46.6\ m^2\ g^{-1}$ to $49.1\ m^2\ g^{-1}$ with the Ag-loading. Our recent study on the sunlight photocatalytic performances of $BiVO_4$ also found that the BET surface area was not the only factor influencing the photocatalytic activities.[107]

Apart from the crystal facet and electronic structures, the existence of surface defects on the photocatalysts remains another important factor affecting its photocatalytic performance. The roles the defects play in the adsorption and surface reactivity have been acknowledged and extensively characterized by various techniques.[132,139,140] Yu *et al.*[132] revealed that more surface hydroxyl groups over the Ag_2CO_3/TiO_2 composite could react with more photo-generated h^+ and produce more $^{\bullet}OH$ radicals to decompose the dye. Zhang *et al.*[139] demonstrated that the visible hydroxyl groups indicated the existence of surface defects on ZnO nanorods, and that the existence of surface defects played a positive role in the photocatalytic activity of ZnO nanorods; whereby, the photo-generated holes could be trapped by surface defects and the separation of photo-generated e^-/h^+ pairs was facilitated. Moreover, the photo-generated holes trapped by surface defects more readily reacted with electron donors and the photocatalytic reaction could thus be greatly promoted; this was the reason why ZnO nanorods with surface defects showed significantly higher photocatalytic performances. Bai *et al.*[140] showed that ZnO_{1-x} with surface oxygen defects could be excited by visible light, due to the narrowing energy band-gap resulting from the generation of the surface defect level induced by the surface oxygen-defect states. The surface defects may serve as adsorption sites as well as charge carrier traps, where the charge transfers to the adsorbed species and prevents the e^-/h^+ recombination. However, TaON nanoparticles with lower surface reduction defect sites exhibited enhanced photocatalytic performance for the mineralization of phenol and its chloro-derivatives in an aqueous phase under visible light irradiation.[37] A possible interpretation of this phenomenon is that the photocatalytic performance may not be governed by a single feature. Therefore, in a diverse photocatalysis system, combined photocatalysts in different combinations and ratios could provide varied results depending upon the conditions used.

4. Application of visible light-responsive photocatalysts in water treatment

Visible light-responsive photocatalysts are expected to play an important role in tackling growing global concerns over water contamination, which is of great significance in alleviating the increasingly serious global water resource crisis. The photocatalysis route itself holds many advantages, such as strong oxidation power, moderate operation temperature, and green-chemistry related procedures, offering a tantalizing route to meet the global challenges associated with the environment, energy, and sustainability, and with the aid of abundant sunlight resources. Visible light-responsive photocatalysts have been widely used for the treatment of inorganic, organic, and biological contaminated water. In this section, the main applications of visible light-responsive photocatalysts in water treatment are briefly summarized, but it is worth noting that most applications discussed here are still in the stage of laboratory research.

4.1. Photocatalytic degradation of organic pollutants

In most cases, different types of dyes are studied as model compounds for the photocatalytic degradation of large organic molecules in water treatment. Organic dyes are often used in textile, printing, and photographic industries, but a sizable fraction of dyes is wasted in the dying process and is released

Table 1 Comparison of the optical properties, band-gap values and BET surface areas of several reported photocatalysts

Photocatalyst	Synthesis method	Optical properties and band-gap	BET surface area ($m^2\ g^{-1}$)	Pollutant	Degradation efficiency or reaction rate	Crystalline phase	Ref.
WO_3–TiO_2/AC	Sol–gel	—	323	10 mg L^{-1}	62.52%	Anatase	53
			357	Congo red	65.76%		
			386		64.91%		
			413		73.28%		
			456		75.34%		
			439		71.16%		
			514		79.35%		
			542		82.21%		
			498		81.46%		
C-doped Bi_2O_3	Calcination	Visible light absorption band around 450–530 nm, the absorption edge of the C-doped Bi_2O_3 has an obvious red-shift compared with the pure Bi_2O_3	5.9	13 mg L^{-1}	95%	Monoclinic	61
Bi_2O_3			1.7	methyl orange	42%		
TiO_2	Hydrothermal	TiO_2 nanotubes absorbed moderately around 385 nm and strongly around 300–350 nm, the optical absorption of Pt–TiO_2 was enhanced significantly in the region of 300–700 nm. The band-gap of the TiO_2 and Pt–TiO_2 were calculated to be TiO_2 (3.16 eV), 0.1 mol% Pt–TiO_2 (3.11 eV), 0.5 mol% Pt–TiO_2 (3.05 eV), 1 mol% Pt–TiO_2 (3.01 eV), 2 mol% Pt–TiO_2 (2.96 eV), 4 mol% Pt–TiO_2 (2.64 eV)	261.7	Acetaldehyde	0.0005 min^{-1}	Anatase	66
0.1 mol% Pt–TiO_2			226.7		0.0028 min^{-1}		
0.5 mol% Pt–TiO_2			203.9		0.0034 min^{-1}		
1 mol% Pt–TiO_2			163.6		0.0012 min^{-1}		
2 mol% Pt–TiO_2			141.8		0.0009 min^{-1}		
4 mol% Pt–TiO_2			139.9		0.0005 min^{-1}		
C–N–TiO_2 (N(0))	Microwave-assisted solvothermal reaction	Compared with those of commercial P25 powders, the absorption edges of the prepared samples apparently shifted to the visible range. The band-gap energies deduced from the tangent line are 3.16, 3.11, 2.98, 2.85, and 2.77 eV for P25, N(0), DEA, TMA, and DETA, respectively	59.0	5 mg L^{-1} RhB	48%, 0.0049 min^{-1}	Anatase	69
C–N–TiO_2 (DEA)			69.7		59%, 0.0142 min^{-1}		
C–N–TiO_2 (TMA)			63.7		92%, 0.0397 min^{-1}		
C–N–TiO_2 (DETA)			129.1		10%, 0.0017 min^{-1}		
TiO_2	Acid catalysed sol–gel	TiO_2 showed an absorption threshold at 406 nm and a band-gap energy of 3.05 eV; N–TiO_2 showed a slight red-shift, giving a band-gap of 3.02 eV; N–Pt–TiO_2 had the longest absorption edge and the highest absorbance in the visible light region, giving a band-gap of 2.58 eV	46.6	20 mg L^{-1} phenol	35.6%	Anatase	70
N–TiO_2			78.5		41.9%		
N–Pt–TiO_2			94.5		100%		
ZnO	Hybridized interaction	Both ZnO and C_{60}–ZnO showed the absorbance edge from 400 nm to 800 nm, the absorption intensity changed with the increasing of the C_{60} amount	57.3	3 mg L^{-1} MB	85%, 0.0337 min^{-1}	Hexagonal	86
C_{60}–ZnO			56.9		95%, 0.0569 min^{-1}		
4.9 wt% g-C_3N_4–ZnO	Calcination	The absorption edges of g-C_3N_4–ZnO composite samples shift significantly to longer wavelengths compared to ZnO, as well as the band-gap narrowing	36	3 mg L^{-1} methyl orange or *p*-nitrophenol	15.6 wt% g-C_3N_4–ZnO exhibited the best photocatalytic performance	Both ZnO and g-C_3N_4 phases	96
8.4 wt% g-C_3N_4–ZnO			75				
15.6 wt% g-C_3N_4–ZnO			33				
58.1 wt% g-C_3N_4–ZnO			28				

Table 1 (*Contd.*)

Photocatalyst	Synthesis method	Optical properties and band-gap	BET surface area ($m^2\ g^{-1}$)	Pollutant	Degradation efficiency or reaction rate	Crystalline phase	Ref.
A-$BiVO_4$ (pH = 4.9)	Hydrothermal	The absorption edges for both the A-$BiVO_4$ and S-$BiVO_4$ samples blue shift eventually as the pH values of the precursors increase. As for A-$BiVO_4$, the absorption edge is measured to be at approx. 560 nm (pH 4.9), 555 nm (pH 6.26), and 540 nm (pH 7); as 590 nm (pH 4.9), 540 nm (pH 6.26), and 525 nm (pH 7) for S-$BiVO_4$. The estimated band-gap energies of A-$BiVO_4$ were approx. 2.40 eV (pH 4.9), 2.43 eV (pH 6.26), and 2.45 eV (pH 7), respectively, whereas for S-$BiVO_4$, the band-gap energies were measured to be approx. 2.28 eV (pH 4.9), 2.40 eV (pH 6.26), and 2.45 eV (pH 7)	10.3	5 mg L^{-1} RhB	61%	Monoclinic scheelite	107
A-$BiVO_4$ (pH = 6.26)			4.6		89%		
A-$BiVO_4$ (pH = 7)			1.6		62%		
S-$BiVO_4$ (pH = 4.9)			6.3		97%		
S-$BiVO_4$ (pH = 6.26)			4.6		96%		
S-$BiVO_4$ (pH = 7)			11.1		61%		

into effluent water streams. In general, the presence of even low concentrations of dyes in effluent streams seriously affects the nature of water, and is difficult to be biodegraded or oxidized with the aid of chemicals. Therefore, appreciable efforts have been made to develop photocatalysts to degrade dyes in aqueous solutions under visible light.[141–143] Bismuth titanate ($Bi_{12}TiO_{20}$) nanostructures with different morphologies have been used to photocatalytically remove acid orange 7 under visible light irradiation, with tests showing that $Bi_{12}TiO_{20}$ has a higher photocatalytic activity than that of traditional N-doped TiO_2; in this regard, the BET surface area plays an important role in the reaction efficiency, while the crystallinity of the samples is another important factor that could also boost the photocatalytic performances.[51] The photosensitization of photocatalysts by dyes has also been used for the visible photodegradation and mineralization of dye pollutants. Li *et al.*[141] initiated a comparison study of dye photodegradation over TiO_2 and ZnO, where the microscale ZnO exhibited much higher visible photocatalytic activity than that of P25, due to the higher photosensitization efficiency of electron transfer from an excited dye to the CB of the microscale ZnO than that of P25. The better crystallinity and lower defects of the microscale ZnO than that of the nanosized ZnO resulted in a better photostability. TiO_2-modified ZnO was developed as a novel light-to-electricity conversion device, and has proven to be a promising candidate for the photocatalytic removal of dye pollutants, as well as a renewable energy source.

Pharmaceutical and personal care products (PPCPs) have recently been considered as emerging contaminants, and are an extraordinarily diverse group of chemicals used in prescription and nonprescription drugs, human health and cosmetic care, veterinary medicine, and agricultural practice.[144] Specific PPCPs may cause ecological harm, such as endocrine disruption and antimicrobial resistance, thus some of PPCPs have been classified as "priority pollutants" by both the US Environmental Protection Agency and the European Union Water Framework Directive. PPCPs have frequently been studied with respect to environmental protection because of their toxicity and non-biodegradability. To date, visible light photocatalytic degradation has been considered as a promising approach for the environmentally friendly decomposition of PPCPs, offering high efficiency, cost effectiveness, ease of operation, *etc.* For example, An and Zhou[145] employed a new combined catalyst copper-plating iron-doped Cu_2O (FeCu/Cu_2O) to degrade a mixture of five commonly used PPCPs (sulfamethoxazole, oxytetracyclin, paracetamol, aspirin, and triclosan) under visible light irradiation. Compared with the Fe/C inner micro-circuit, the electric currents flowing between Cu and Fe increased the speed of anodic Fe dissolution. It was found that Cu_2O could accelerate the PPCP degradation processes under visible light irradiation, due to its photochemical properties. Moreover, the increased dissolved oxygen concentration in the solution by shaking not only preconditioned the photo-catalysis reaction, but also set the stage for Fe reduction. Zhao *et al.*[146] investigated the photochemical degradation of the antibiotic oxytetracycline (OTC) with nitrogen- and fluorine-doped titanium dioxide (NF–TiO_2) film at different pH values in aqueous solutions

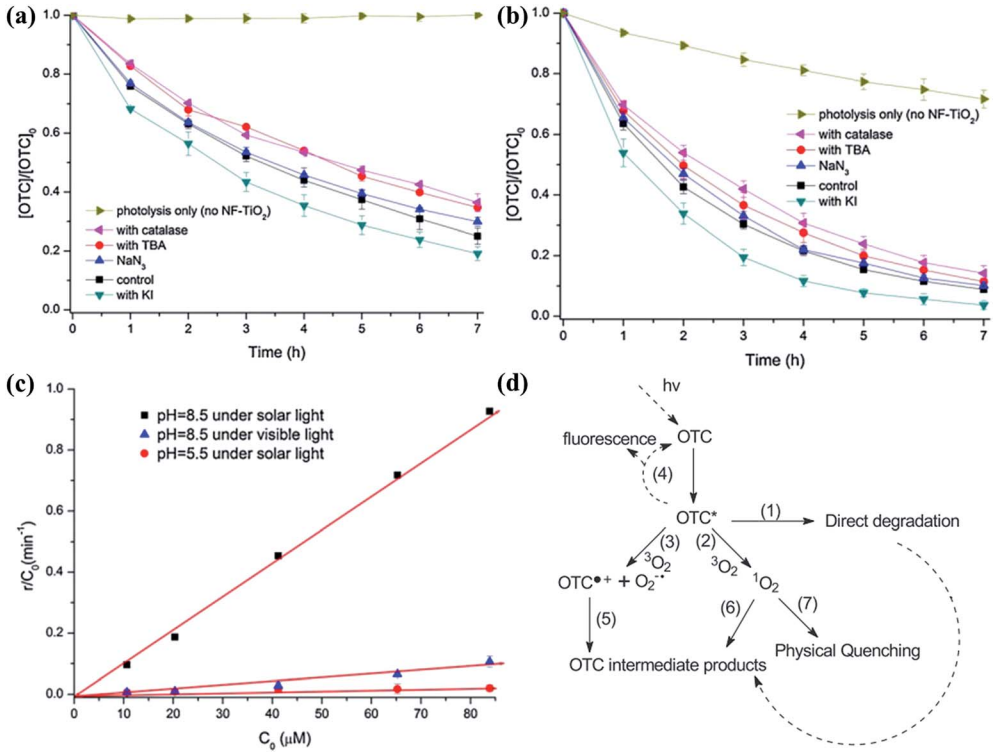

Fig. 5 Influence of TBA (10 mM), NaN_3 (5 mM), KI (10 mM) and catalase (6 unit per L) on the photocatalytic degradation of OTC by NF–TiO_2 under visible light at pH 5.5 (a) and 8.5 (b) (OTC 5 mg L^{-1}). (c) The initial rate of OTC photolytic degradation per unit of concentration at various initial concentrations at pH 5.5 and 8.5 under visible and solar light. (d) The proposed pathway of OTC photolytic degradation. Reproduced with permission from ref. 146.

under visible and solar light irradiation. The kinetics and mechanism during the photolytic and photocatalytic degradation of OTC were intensively studied. The photochemical degradation of OTC with NF–TiO_2 film could occur *via* a number of competing reaction processes, such as direct photolytic degradation, as shown in Fig. 5; whereby, the electrons and holes could be separated by the excited NF–TiO_2 under light irradiation, followed by the fact that a series of active redox species were produced by a series of reactions, leading to the oxidative-reductive degradation of OTC.

Phenolic compounds can cause various diseases, including cancer, angiocardiopathy, and gastroenterology *etc.*, even at very low concentrations, and represent a typical family of organic pollutants widely present in wastewater from petrol, coal, and other chemical industries.[147] Most phenolic compounds are usually difficult to be mineralized by a biodegradation method, due to the stable benzene ring and its recalcitrant nature. However, such compounds have been reported to be effectively degraded by visible light-responsive photocatalysts.[30,37,79,127,147] Li and colleagues[147] synthesized a novel layered perovskite crystal La_2NiO_4 photocatalyst with high activity for mineralizing 4-chlorophenol under visible light irradiation. First, the 4-chlorophenol was ionized into anions and donated electrons to La_2NiO_4 due to its positively charged surface. Then, the electrons could react with dissolved O_2 to produce $^{\bullet}O_2^-$ radicals, followed by reacting with H^+ to form $^{\bullet}OH$ radicals, which could oxidize 4-chlorophenol into CO_2, thus leading to complete degradation. Other organic pollutions, such as benzyl alcohol,[148] methanol,[149] benzyl amine,[150] hydroxytyrosol,[151] and benzene,[152] in aqueous solutions have also been reported to be efficiently degraded by visible light induced photocatalytic.

4.2. Photocatalytic degradation of inorganic pollutants

The presence of inorganic impurities, such as residual ions and acids, in the water matrix has distinctive effects toward a water system's ecological environment. Some of them are highly toxic to most of living organisms when their concentration levels are higher than a certain value. For instance, hexavalent chromium (Cr(VI)) is a carcinogenic and mutagenic pollutant, which is frequently found in wastewater, possibly stemming from pigment production, metal plating, and leather tanning, *etc.* The visible light induced photocatalytic reduction of aqueous Cr(VI) has received much attention recently, due to its low cost and high efficiency without secondary pollution.[153,154] For instance, synthesized $SnIn_4S_8$ particles with a flower-like nanostructure could exhibit an excellent photocatalytic reduction efficiency of aqueous Cr(VI) (~97%) and good photocatalytic stability.[153] The strong absorption in the visible light region, large surface area, and excellent charge separation characteristics of $SnIn_4S_8$ are responsible for its promising removal performance. The mechanism for Cr(VI) removal from water by $SnIn_4S_8$ is shown in Fig. 6. The photo-generated electrons in the VB of $SnIn_4S_8$ could be excited to the CB, while holes are then generated in the VB. Subsequently, a portion of

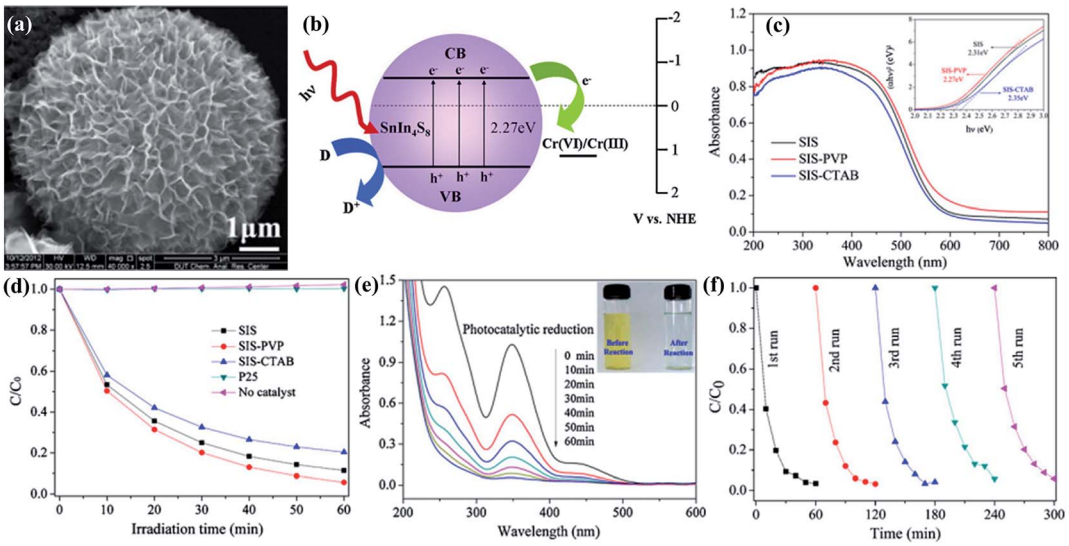

Fig. 6 (a) SEM image of $SnIn_4S_8$ nanostructure. (b) Schematic diagram for the photocatalytic reduction of Cr(VI) ions by $SnIn_4S_8$ under visible light irradiation. (c) UV-vis diffuse reflectance spectra of the samples SIS, SIS-PVP and SIS-CTAB. Inset: plots of $(Ah\nu)^2$ *versus* $h\nu$ for calculating the band-gap energy. (d) Comparison of the photocatalytic reduction of aqueous Cr(VI) over the as-prepared samples and the commercial P25 TiO_2 under visible light irradiation. (e) UV-vis absorbance spectrum of $K_2Cr_2O_7$ solution in the presence of SIS-PVP products under visible light irradiation. The inset shows the digital images of the solution before and after reaction. (f) The photocatalytic reduction of aqueous Cr(VI) over the sample SIS-PVP with five times cycling use. Reproduced with permission from ref. 153.

the photo-generated e^-–h^+ pairs migrate to the surface of the $SnIn_4S_8$ and participate in the redox reaction. The photo-generated e^- reduces the adsorbed Cr(VI) to Cr(III), while the h^+ enables the oxidization of water to O_2. By this means, the photocatalytic reduction of Cr(VI) coupled with the synergistic effect of photo-degradation of bisphenol A in aqueous solution is also achieved by using Bi_2O_3/TiO_2 under visible light irradiation.[154]

4.3. Photocatalytic disinfection of biological pollutants

The different types of microbes (bacteria, viruses, fungi, algae, plankton, *etc.*) present in wastewater are harmful to health and can cause various diseases.[155] Over the past few decades, the visible light activated photocatalytic disinfection of water has received significant attention, with research focus moving from laboratory studies to potential applications.[156,157] For example, a dye-sensitized TiO_2 thin film was used in the photocatalytic disinfection of phytopathogenic bacteria under visible light irradiation. The inhibition rates of *Erwinia carotovora subsp. carotovora* 3, *Enterobacter cloacae* SM1, and *E. carotovora subsp. carotovora* 7 that could induce severe soft/basal rot disease in vegetable crops were higher than 90%. These results indicated that the visible light-responsive dye-sensitized TiO_2 thin film had the potential for direct application to plant protection in water systems.[156] A visible light-activated palladium-modified nitrogen-doped titanium oxide (TiON/PdO) photocatalyst has been demonstrated with good visible light adsorption and a superior efficient photocatalytic disinfection effect on Fungi *Fusarium graminearum* macroconidia. The disinfection effect benefitted from the strong adsorption of the TiON/PdO photocatalyst onto the *Fusarium graminearum* macroconidia surface

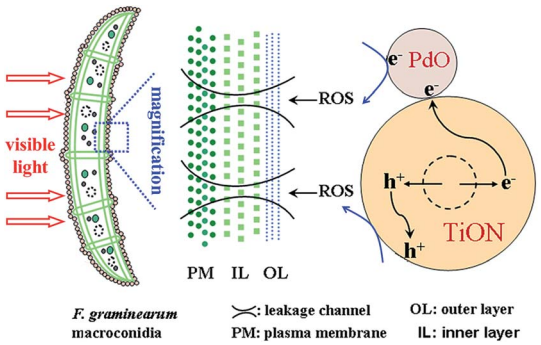

Fig. 7 Photocatalytic disinfection mechanism of TiON/PdO photocatalyst on *Fusarium graminearum* macroconidia under visible light irradiation. Reproduced with permission from ref. 157, copyright (2013) American Chemical Society.

due to their opposite surface charges. The photocatalytic disinfection mechanism of the TiON/PdO photocatalyst on the *Fusarium graminearum* macroconidia is displayed in Fig. 7, and is attributed to their cell wall/membrane damage caused by the attack from the reactive oxygen species (ROSs), while a breakage of their cell structure was not necessary for their loss of viability.[157]

5. Conclusion and perspectives

Visible light-responsive photocatalysis for water and wastewater treatment is gaining momentum globally and presenting great opportunities to revolutionize water and wastewater treatment due to its unique features. In this review, we have extensively reviewed the current progress in heterogeneous

photocatalytic water treatment using visible light-responsive photocatalysts. The fundamentals of heterogeneous photocatalysis and the regulatory mechanism of visible light-responsive photocatalysis, as well as the unique features of visible light-responsive photocatalysts have been briefly discussed. To extend the optical response of photocatalysts into the visible region, a variety of methods, such as the modification of traditional photocatalysts *via* doping, dye sensitization, formation of a heterostructure, coupled with π-conjugated structure, and exploration of novel multi-component oxides and nanocomposites with visible light responses, have been developed. These photocatalysts have been widely used for the degradation of inorganic and organic pollutants, as well as for photocatalytic disinfection. Therefore, these results show promise for the further development of sustainable environmental remediation technologies based on photocatalytic redox reactions driven by visible light as a renewable source of energy.

Although steady progress in heterogeneous photocatalytic water treatment using visible light-responsive photocatalysts has been achieved,[158] studies in this field are still at the immature stage and further developments are required. The challenges faced in developing water treatment with visible light-responsive photocatalysts are significant, but many are perhaps only temporary including the high cost, technical hurdles, and potential environmental and human risks. To promote the feasibility of visible light-responsive photocatalytic water treatment technology in the near future, several key technical constraints, ranging from catalyst development to reactor design and process optimization, have to be addressed including the following specific aspects:

(i) Improving the efficiency and photo-stability of the visible light-responsive photocatalysts. The performance of visible light-responsive photocatalysts is currently limited by the physicochemical properties of these materials. For example, among the modification methods, though dye sensitization has been able to extend the adsorption light wavelength to the visible light range and improve the activity of traditional photocatalysts under visible light, the usage of such photocatalytic materials is still limited due to issues regarding the dissolution and degradation of dyes, which retards their photocatalysis applications. Therefore, a more careful design of the functional photocatalyst is required to obtain suitable physicochemical properties of the materials.

(ii) Devising an appropriate photocatalyst immobilization strategy to provide a cost-effective solid–liquid separation. One detrimental limitation at the current stage is running-out of the catalyst during the photocatalytic process, which jeopardizes the regeneration of the catalysts and poses adverse impacts on the environment due to the leakage of the photocatalyst. Immobilized photocatalytic systems can avoid problems associated with catalyst recovery and agglomeration, as well as minimizing the scale of the reactor.

(iii) Designing an effective photoreactor for the full utilization of solar energy to reduce the electricity costs. The implementation of photocatalytic processes at an industrial level requires the design of suitable photoreactors, where a proper design and build-up of such devices would be helpful to better harvest solar energy, accommodate the photocatalysts and reactants, as well as collect the reaction products.

(iv) Establishing a globally experimental database regarding the information of the photocatalysts tested including the types of catalyst materials, preparation routes, modifications, photocatalytic reaction environments and activity. Such a database should be easily accessible to avoid any repeated, unnecessary work and should guide the development of innovative catalysts. To obtain the desired photo-degradation efficiency, combining different techniques and approaches might always be indispensable. In this regard, a database detailing the fabrication and usage of the existing photocatalysts needs to be established because plenty of nanostructured materials have already been used in visible light-responsive photocatalysis. The accumulation of a large amount of theoretical and modelling work is also useful and imperative in the quest to foster a deep understanding of the preparation, properties and performances of photocatalysts and their optimization for water treatment. Multi-technology integration will provide a bright prospect for water treatment and energy-related issues using visible light-responsive photocatalysts with advanced efficiency and good robustness.

Acknowledgements

The authors are grateful for the financial support from the Key Science and Technology Program of Henan Province, PR China (Grant nos 122102310486 and 132102210129), the Basic Scientific and Technological Frontier Project of Henan Province, PR China (Grant nos 102300410098, 132330410138, and 122300410293). The authors also would like to thank the Innovation Scientists and Technicians Troop Construction Projects of Henan Province, the Plan for Scientific Innovation Talent of Henan Province (Grant no. 134200510014), the Fostering Foundation of Henan Normal University for the Author of National Excellent Ph.D. Dissertation, PR China (Grant no. 01333900011), and the National Natural Science Foundation of China (Grants no. 21477034).

References

1 J. Qu and M. Fan, *Crit. Rev. Environ. Sci. Technol.*, 2010, **40**, 519–560.
2 X. Zhou, Y. Li and Y. Zhao, *RSC Adv.*, 2014, **30**, 15620–15629.
3 V. K. Gupta, I. Ali, T. A. Saleh, A. Nayak and S. Agarwal, *RSC Adv.*, 2012, **2**, 6380–6388.
4 J. Sun, B. Zhang, R. Sun, Y. Li and J. Wu, *Int. J. Environ. Pollut.*, 2009, **38**, 81–87.
5 S. Sun, C. Li, J. Sun, S. Shi, M. Fan and Q. Zhou, *J. Hazard. Mater.*, 2009, **161**, 1052–1057.
6 J. Sun, S. Sun, M. Fan, H. Guo, Y. Lee and R. Sun, *J. Hazard. Mater.*, 2008, **153**, 187–193.
7 O. Ganzenko, D. Huguenot, E. D. van Hullebusch, G. Esposito and M. A. Oturan, *Environ. Sci. Pollut. Res.*, 2014, **21**, 8493–8524.

8 S. Ray, M. Takafuji and H. Ihara, *RSC Adv.*, 2013, **3**, 23664–23672.
9 M. Tanveer and G. T. Guyer, *Renewable Sustainable Energy Rev.*, 2013, **24**, 534–543.
10 L. Yang, S. Dong, J. Sun, J. Feng, Q. Wu and S. Sun, *J. Hazard. Mater.*, 2010, **179**, 438–443.
11 P. Fageria, S. Gangopadhyay and S. Pande, *RSC Adv.*, 2014, **4**, 24962–24972.
12 S. Balachandran, S. G. Praveen, R. Velmurugan and M. Swaminathan, *RSC Adv.*, 2014, **4**, 4353–4362.
13 Y. C. Chang, *RSC Adv.*, 2014, **4**, 20273–20280.
14 L. G. Devi and R. Kavitha, *Appl. Catal., B*, 2013, **140**, 559–587.
15 D. Kanakaraju, B. D. Glass and M. Oelgemoeller, *Environ. Chem. Lett.*, 2014, **12**, 27–47.
16 A. Rey, P. Garcia-Munoz, M. D. Hernandez-Alonso, E. Mena, S. Garcia-Rodriguez and F. J. Beltran, *Appl. Catal., B*, 2014, **154**, 274–284.
17 J. Sun, L. Qiao, S. Sun and G. Wang, *J. Hazard. Mater.*, 2008, **155**, 312–319.
18 Z. Li, Y. Fang and S. Xu, *Mater. Lett.*, 2013, **93**, 345–348.
19 L. Z. Qin, H. Liang, B. Liao, A. D. Liu, X. Y. Wu and J. Sun, *Nucl. Instrum. Methods Phys. Res., Sect. B*, 2013, **307**, 385–390.
20 Y. Min, K. Zhang, Y. Chen and Y. Zhang, *Chem. Eng. J.*, 2011, **175**, 76–83.
21 Q. Li, L. Zong, Y. Xing, X. Wang, L. Yu and J. Yang, *Sci. Adv. Mater.*, 2013, **5**, 1316–1322.
22 B. Ohtani, *J. Photochem. Photobiol., C*, 2010, **11**, 157–178.
23 C. Mondal, M. Ganguly, J. Pal, A. Roy, J. Jana and T. Pal, *Langmuir*, 2014, **30**, 4157–4164.
24 W. Wang, J. Wang, Z. Wang, X. Wei, L. Liu, Q. Ren, W. Gao, Y. Liang and H. Shi, *Dalton Trans.*, 2014, **43**, 6735–6743.
25 S. Zhang, *Ceram. Int.*, 2014, **40**, 4553–4557.
26 Z. Li, S. Yang, J. Zhou, D. Li, X. Zhou, C. Ge and Y. Fang, *Chem. Eng. J.*, 2014, **241**, 344–351.
27 S. Wang, D. Li, C. Sun, S. Yang, Y. Guan and H. He, *J. Mol. Catal. A: Chem.*, 2014, **383**, 128–136.
28 H. Huang, Y. Feng, J. Zhou, G. Li and K. Dai, *Desalin. Water Treat.*, 2013, **51**, 7236–7240.
29 H. Cheng, B. Huang and Y. Dai, *Nanoscale*, 2014, **6**, 2009–2026.
30 J. Sheng, X. Li and Y. Xu, *ACS Catal.*, 2014, **4**, 732–737.
31 Y. S. Xu, Y. X. Yu and W. D. Zhang, *J. Nanosci. Nanotechnol.*, 2014, **14**, 6800–6808.
32 U. M. Garcia-Perez, A. Martinez-de la Cruz and J. Peral, *Electrochim. Acta*, 2012, **81**, 227–232.
33 S. Dong, J. Sun, Y. Li, C. Yu, Y. Li and J. Sun, *Appl. Catal., B*, 2014, **144**, 386–393.
34 M. Shang, W. Wang, L. Zhou, S. Sun and W. Yin, *J. Hazard. Mater.*, 2009, **172**, 338–344.
35 T. Li, L. Zhao, Y. He, J. Cai, M. Luo and J. Lin, *Appl. Catal., B*, 2013, **129**, 255–263.
36 L. Armelao, D. Barreca, G. Bottaro, A. Gasparotto, C. Maccato, C. Maragno, E. Tondello, U. L. Stangar, M. Bergant and D. Mahne, *Nanotechnology*, 2007, **18**, 375709.
37 Y. Chen, S. Liang, L. Wen, W. Wu, R. Yuan, X. Wang and L. Wu, *Phys. Chem. Chem. Phys.*, 2013, **15**, 12742–12747.
38 D. Barreca, A. P. Ferrucci, A. Gasparotto, C. Maccato, C. Maragno and E. Tondello, *Chem. Vap. Deposition*, 2007, **13**, 618–625.
39 L. Armelao, D. Barreca, G. Bottaro, A. Gasparotto, C. Maccato, E. Tondello, O. I. Lebedev, S. Turner, G. Van Tendeloo, C. Sada and U. L. Stangar, *ChemPhysChem*, 2009, **10**, 3249–3259.
40 G. Carraro, R. Sugrañez, C. Maccato, A. Gasparotto, D. Barreca, C. Sada, M. Cruz-Yusta and L. Sánchez, *Thin Solid Films*, 2014, **564**, 121–127.
41 A. Abd Aziz, C. K. Cheng, S. Ibrahim, M. Matheswaran and P. Saravanan, *Chem. Eng. J.*, 2012, **183**, 349–356.
42 M. N. Chong, B. Jin, C. W. K. Chow and C. Saint, *Water Res.*, 2010, **44**, 2997–3027.
43 E. Casbeer, V. K. Sharma and X. Z. Li, *Sep. Purif. Technol.*, 2012, **87**, 1–14.
44 Y. Qu and X. Duan, *Chem. Soc. Rev.*, 2013, **42**, 2568–2580.
45 C. Chen, W. Ma and J. Zhao, *Chem. Soc. Rev.*, 2010, **39**, 4206–4219.
46 R. Abe, *J. Photochem. Photobiol., C*, 2010, **11**, 179–209.
47 K. Mori and H. Yamashita, *Phys. Chem. Chem. Phys.*, 2010, **12**, 14420–14432.
48 X. Qu, P. J. J. Alvarez and Q. Li, *Water Res.*, 2013, **47**, 3931–3946.
49 X. G. Yan, L. Xu, W. Q. Huang, G. F. Huang, Z. M. Yang, S. Q. Zhan and J. P. Long, *Mater. Sci. Semicond. Process.*, 2014, **23**, 34–41.
50 L. Gu, J. Wang, Z. Zou and X. Han, *J. Hazard. Mater.*, 2014, **268**, 216–223.
51 X. Zhu, J. Zhang and F. Chen, *Chemosphere*, 2010, **78**, 1350–1355.
52 J. Sun, S. Dong, Y. Wang and S. Sun, *J. Hazard. Mater.*, 2009, **172**, 1520–1526.
53 J. Sun, Y. Wang, R. Sun and S. Dong, *Mater. Chem. Phys.*, 2009, **115**, 303–308.
54 R. Asahi, T. Morikawa, T. Ohwaki, K. Aoki and Y. Taga, *Science*, 2001, **293**, 269–271.
55 G. Liu, L. Wang, H. G. Yang, H.-M. Cheng and G. Q. Lu, *J. Mater. Chem.*, 2010, **20**, 831–843.
56 C. Di Valentin and G. Pacchioni, *Catal. Today*, 2013, **206**, 12–18.
57 W. J. Ong, L. L. Tan, S. P. Chai, S. T. Yong and A. R. Mohamed, *Nanoscale*, 2014, **6**, 1946–2008.
58 Y. Wang, C. Feng, M. Zhang, J. Yang and Z. Zhang, *Appl. Catal., B*, 2010, **100**, 84–90.
59 B. Neumann, P. Bogdanoff, H. Tributsch, S. Sakthivel and H. Kisch, *J. Phys. Chem. B*, 2005, **109**, 16579–16586.
60 Y. J. Chen, G. Y. Jhan, G. L. Cai, C. S. Lin, M. S. Wong, S. C. Ke, H. H. Lo, C. L. Cheng and J. J. Shyue, *J. Vac. Sci. Technol., A*, 2010, **28**, 779–782.
61 G. Dai, S. Liu and Y. Liang, *J. Alloys Compd.*, 2014, **608**, 44–48.
62 M. Samadi, H. A. Shivaee, M. Zanetti, A. Pourjavadi and A. Moshfegh, *J. Mol. Catal. A: Chem.*, 2012, **359**, 42–48.
63 R. Leary and A. Westwood, *Carbon*, 2011, **49**, 741–772.
64 M. Pelaez, N. T. Nolan, S. C. Pillai, M. K. Seery, P. Falaras, A. G. Kontos, P. S. M. Dunlop, J. W. J. Hamilton,

J. A. Byrne, K. O'Shea, M. H. Entezari and D. D. Dionysiou, *Appl. Catal., B*, 2012, **125**, 331–349.
65 J. Li, J. Xu and J. Huang, *CrystEngComm*, 2014, **16**, 375–384.
66 B. K. Vijayan, N. M. Dimitrijevic, J. Wu and K. A. Gray, *J. Phys. Chem. C*, 2010, **114**, 21262–21269.
67 J. Sun, S. Dong, J. Feng, X. Yin and X. Zhao, *J. Mol. Catal. A: Chem.*, 2011, **335**, 145–150.
68 H. F. Moafi, M. A. Zanjanchi and A. F. Shojaie, *J. Nanosci. Nanotechnol.*, 2014, **14**, 7139–7150.
69 Y. C. Wu and L. S. Ju, *J. Alloys Compd.*, 2014, **604**, 164–170.
70 H. Sun, G. Zhou, S. Liu, H. M. Ang, M. O. Tade and S. Wang, *Chem. Eng. J.*, 2013, **231**, 18–25.
71 J. Zhao, C. Chen and W. Ma, *Top. Catal.*, 2005, **35**, 269–278.
72 Z. Li, Y. Fang, X. Zhan and S. Xu, *J. Alloys Compd.*, 2013, **564**, 138–142.
73 D. Chatterjee and S. Dasgupta, *J. Photochem. Photobiol., C*, 2005, **6**, 186–205.
74 J. Shang, F. Zhao, T. Zhu and J. Li, *Sci. China: Chem.*, 2011, **54**, 167–172.
75 X. Li, Y. Cheng, S. Kang and J. Mu, *Appl. Surf. Sci.*, 2010, **256**, 6705–6709.
76 G. C. C. Yang and S. W. Chan, *J. Nanopart. Res.*, 2009, **11**, 221–230.
77 J. Li, Z. Guo, Y. Wang and Z. Zhu, *Micro Nano Lett.*, 2014, **9**, 65–68.
78 Y. Wu, F. Xu, D. Guo, Z. Gao, D. Wu and K. Jiang, *Appl. Surf. Sci.*, 2013, **274**, 39–44.
79 W. Teng, X. Li, Q. Zhao and G. Chen, *J. Mater.Chem. A*, 2013, **1**, 9060–9068.
80 M. Lee and K. Yong, *Nanotechnology*, 2012, **23**, 194014.
81 Z. Wei, Y. Li, S. Luo, C. Liu, D. Meng, M. Ding and G. Zeng, *Sep. Purif. Technol.*, 2014, **122**, 60–66.
82 W. Zhou, Y. Guan, D. Wang, X. Zhang, D. Liu, H. Jiang, J. Wang, X. Liu, H. Liu and S. Chen, *Chem.–Asian J.*, 2014, **9**, 1648–1654.
83 Y. Ni, W. Wang, W. Huang, C. Lu and Z. Xu, *J. Colloid Interface Sci.*, 2014, **428**, 162–169.
84 R. T. Thomas, P. Abdul Rasheed and N. Sandhyarani, *J. Colloid Interface Sci.*, 2014, **428**, 214–221.
85 Q. J. Xiang, J. G. Yu and M. Jaroniec, *Chem. Soc. Rev.*, 2012, **41**, 782–796.
86 H. Fu, T. Xu, S. Zhu and Y. Zhu, *Environ. Sci. Technol.*, 2008, **42**, 8064–8069.
87 Y. Long, Y. Lu, Y. Huang, Y. Peng, Y. Lu, S. Z. Kang and J. Mu, *J. Phys. Chem. C*, 2009, **113**, 13899–13905.
88 D. Chen, K. Wang, D. Xiang, R. Zong, W. Yao and Y. Zhu, *Appl. Catal., B*, 2014, **147**, 554–561.
89 F. Wang, S. Min, Y. Han and L. Feng, *Superlattices Microstruct.*, 2010, **48**, 170–180.
90 X. Li, D. Wang, G. Cheng, Q. Luo, J. An and Y. Wang, *Appl. Catal., B*, 2008, **81**, 267–273.
91 F. Deng, L. Min, X. Luo, S. Wu and S. Luo, *Nanoscale*, 2013, **5**, 8703–8710.
92 Y. Min, K. Zhang, W. Zhao, F. Zheng, Y. Chen and Y. Zhang, *Chem. Eng. J.*, 2012, **193–194**, 203–210.
93 S. Gayathri, P. Jayabal, M. Kottaisamy and V. Ramakrishnan, *J. Appl. Phys.*, 2014, 115.
94 S. Dong, Y. Li, J. Sun, C. Yu, Y. Li and J. Sun, *Mater. Chem. Phys.*, 2014, **145**, 357–365.
95 T. Hasobe, S. Hattori, P. V. Kamat and S. Fukuzumi, *Tetrahedron*, 2006, **62**, 1937–1946.
96 J. X. Sun, Y. P. Yuan, L. G. Qiu, X. Jiang, A. J. Xie, Y. H. Shen and J. F. Zhu, *Dalton Trans.*, 2012, **41**, 6756.
97 M. Fu, J. Liao, F. Dong, H. Li and H. Liu, *J. Nanomater.*, 2014, **2014**, 1–8.
98 Q. Luo, L. Bao, D. Wang, X. Li and J. An, *J. Phys. Chem. C*, 2012, **116**, 25806–25815.
99 F. F. Li, D. F. Yang, M. S. Xia, Y. Wang and Y. S. Jiang, *J. Inorg. Mater.*, 2011, **26**, 917–922.
100 J. Y. Zheng, S. H. Bao, Y. Guo and P. Jin, *ACS Appl. Mater. Interfaces*, 2014, **6**, 5940–5946.
101 G. Chen, M. Sun, Q. Wei, Y. Zhang, B. Zhu and B. Du, *J. Hazard. Mater.*, 2013, **244**, 86–93.
102 Y. C. Nah, I. Paramasivam and P. Schmuki, *ChemPhysChem*, 2010, **11**, 2698–2713.
103 X. Chen, L. Liu, P. Y. Yu and S. S. Mao, *Science*, 2011, **331**, 746–750.
104 J. Su, Y. Zhang, S. Xu, S. Wang, H. Ding, S. Pan, G. Wang, G. Li and H. Zhao, *Nanoscale*, 2014, **6**, 5181–5192.
105 F. Duan, Q. Zhang, Q. Wei, D. Shi and M. Chen, *Prog. Chem.*, 2014, **26**, 30–40.
106 P. Madhusudan, J. Yu, W. Wang, B. Cheng and G. Liu, *Dalton Trans.*, 2012, **41**, 14345–14353.
107 S. Dong, J. Feng, Y. Li, L. Hu, M. Liu, Y. Wang, Y. Pi, J. Sun and J. Sun, *Appl. Catal., B*, 2014, **152**, 413–424.
108 S. Dong, C. Yu, Y. Li, Y. Li, J. Sun and X. Geng, *J. Solid State Chem.*, 2014, **211**, 176–183.
109 C. Yu, S. Dong, J. Feng, J. Sun, L. Hu, Y. Li and J. Sun, *Environ. Sci. Pollut. Res.*, 2014, **21**, 2837–2845.
110 L. Hu, S. Dong, Y. Li, Y. Pi, J. Wang, Y. Wang and J. Sun, *J. Taiwan Inst. Chem. Eng.*, 2014, **45**, 2462–2468.
111 X. J. Dai, Y. S. Luo, W. D. Zhang and S. Y. Fu, *Dalton Trans.*, 2010, **39**, 3426–3432.
112 J. Shang, W. Hao, X. Lv, T. Wang, X. Wang, Y. Du, S. Dou, T. Xie, D. Wang and J. Wang, *ACS Catal.*, 2014, **4**, 954–961.
113 J. Ding, S. Sun, J. Bao, Z. Luo and C. Gao, *Catal. Lett.*, 2009, **130**, 147–153.
114 J. W. Tang, Z. G. Zou and J. H. Ye, *Res. Chem. Intermed.*, 2005, **31**, 513–519.
115 Y. Li, S. Dong, Y. Wang, J. Sun, Y. Li, Y. Pi, L. Hu and J. Sun, *J. Mol. Catal. A: Chem.*, 2014, **387**, 138–146.
116 S. Dong, Y. Cui, Y. Wang, Y. Li, L. Hu, J. Sun and J. Sun, *Chem. Eng. J.*, 2014, **249**, 102–110.
117 D. Channei, B. Inceesungvorn, N. Wetchakun and S. Phanichphant, *J. Nanosci. Nanotechnol.*, 2014, **14**, 7756–7762.
118 L. Zhang, W. Wang, S. Sun, D. Jiang and E. Gao, *CrystEngComm*, 2013, **15**, 10043–10048.
119 X. Zhao, H. Liu, Y. Shen and J. Qu, *Appl. Catal., B*, 2011, **106**, 63–68.
120 S. Kant, S. Kalia and A. Kumar, *J. Alloys Compd.*, 2013, **578**, 249–256.
121 C. Singh, S. Bansal and S. Singhal, *Phys. B*, 2014, **444**, 70–76.

122 W. Shi, J. Shi, S. Yu and P. Liu, *Appl. Catal., B*, 2013, **138**, 184–190.
123 W. Du, X. Wang, H. Li, D. Ma, S. Hou, J. Zhang, X. Qian and H. Pang, *J. Am. Ceram. Soc.*, 2013, **96**, 2979–2986.
124 J. M. Song, H. Q. Hu, X. Z. Wang, S. J. Zhao, Y. L. Shi and M. S. Ren, *J. Inorg. Mater.*, 2013, **28**, 1275–1280.
125 B. L. Fei, W. Li, J. H. Wang, Q. B. Liu, J. Y. Long, Y. G. Li, K. Z. Shao, Z. M. Su and W. Y. Sun, *Dalton Trans.*, 2014, **43**, 10005–10012.
126 P. D. Kanhere, J. Zheng and Z. Chen, *J. Phys. Chem. C*, 2011, **115**, 11846–11853.
127 R. Xing, L. Wu, Z. Fei and P. Wu, *J. Environ. Sci.*, 2013, **25**, 1687–1695.
128 V. Štengl, S. Bakardjieva, N. Murafa, V. Houšková and K. Lang, *Microporous Mesoporous Mater.*, 2008, **110**, 370–378.
129 N. Soltani, E. Saion, W. M. M. Yunus, M. Erfani, M. Navasery, G. Bahmanrokh and K. Rezaee, *Appl. Surf. Sci.*, 2014, **290**, 440–447.
130 C. Tan, G. Zhu, M. Hojamberdiev, K. S. Lokesh, X. Luo, L. Jin, J. Zhou and P. Liu, *J. Hazard. Mater.*, 2014, **278**, 572–583.
131 X. Zheng, S. Meng, J. Chen, J. Wang, J. Xian, Y. Shao, X. Fu and D. Li, *J. Phys. Chem. C*, 2013, **117**, 21263–21273.
132 C. Yu, L. Wei, J. Chen, Y. Xie, W. Zhou and Q. Fan, *Ind. Eng. Chem. Res.*, 2014, **53**, 5759–5766.
133 I. S. Cho, D. W. Kim, S. Lee, C. H. Kwak, S. T. Bae, J. H. Noh, S. H. Yoon, H. S. Jung, D. W. Kim and K. S. Hong, *Adv. Funct. Mater.*, 2008, **18**, 2154–2162.
134 K. Ding, B. Chen, Z. Fang and Y. Zhang, *Theor. Chem. Acc.*, 2013, **132**, 1352.
135 X. Wang, G. Liu, Z.-G. Chen, F. Li, G. Q. Lu and H. M. Cheng, *Chem. Lett.*, 2009, **38**, 214–215.
136 H. Guo, Y. Ke, D. Wang, K. Lin, R. Shen, J. Chen and W. Weng, *J. Nanopart. Res.*, 2013, **15**, 1475.
137 S. Liang, R. Liang, L. Wen, R. Yuan, L. Wu and X. Fu, *Appl. Catal., B*, 2012, **125**, 103–110.
138 W. J. Kim, D. Pradhan, B.-K. Min and Y. Sohn, *Appl. Catal., B*, 2014, **147**, 711–725.
139 X. Zhang, J. Qin, Y. Xue, P. Yu, B. Zhang, L. Wang and R. Liu, *Sci. Rep.*, 2014, **4**, 4596.
140 X. Bai, L. Wang, R. Zong, Y. Lv, Y. Sun and Y. Zhu, *Langmuir*, 2013, **29**, 3097–3105.
141 Y. Li, W. Xie, X. Hu, G. Shen, X. Zhou, Y. Xiang, X. Zhao and P. Fang, *Langmuir*, 2010, **26**, 591–597.
142 L. Luo, A. T. Cooper and M. Fan, *J. Hazard. Mater.*, 2009, **161**, 175–182.
143 Y. He, L. Zhang, X. Wang, Y. Wu, H. Lin, L. Zhao, W. Weng, H. Wan and M. Fan, *RSC Adv.*, 2014, **4**, 13610–13619.
144 S. T. Gadge and B. M. Bhanage, *RSC Adv.*, 2014, **4**, 10367–10389.
145 J. An and Q. Zhou, *J. Environ. Sci.*, 2012, **24**, 827–833.
146 C. Zhao, M. Pelaez, X. Duan, H. Deng, K. O'Shea, D. Fatta-Kassinos and D. D. Dionysiou, *Appl. Catal., B*, 2013, **134–135**, 83–92.
147 G. Li, Y. Zhang, L. Wu, F. Wu, R. Wang, D. Zhang, J. Zhu and H. Li, *RSC Adv.*, 2012, **2**, 4822–4828.
148 S. Higashimoto, R. Shirai, Y. Osano, M. Azuma, H. Ohue, Y. Sakata and H. Kobayashi, *J. Catal.*, 2014, **311**, 137–143.
149 A. A. Ismail, L. Robben and D. W. Bahnemann, *ChemPhysChem*, 2011, **12**, 982–991.
150 S. Higashimoto, Y. Hatada, R. Ishikawa, M. Azuma, Y. Sakata and H. Kobayashi, *Curr. Org. Chem.*, 2013, **17**, 2374–2381.
151 H. B. Y. Smida, M. Beicheickh and B. Jamoussi, *J. Residuals Sci. Technol.*, 2013, **10**, 47–54.
152 R. M. Mohamed and E. Aazam, *Desalin. Water Treat.*, 2013, **51**, 6082–6090.
153 L. Wang, X. Li, W. Teng, Q. Zhao, Y. Shi, R. Yue and Y. Chen, *J. Hazard. Mater.*, 2013, **244–245**, 681–688.
154 J. Yang, J. Dai and J. Li, *Environ. Sci. Pollut. Res.*, 2012, **20**, 2435–2447.
155 H. Chen, X. Zheng, Y. Chen and H. Mu, *RSC Adv.*, 2013, **3**, 9835–9842.
156 K. S. Yao, D. Y. Wang, C. Y. Chang, K. W. Weng, L. Y. Yang, S. J. Lee, T. C. Cheng and C. C. Hwang, *Surf. Coat. Technol.*, 2007, **202**, 1329–1332.
157 J. Zhang, Y. Liu, Q. Li, X. Zhang and J. K. Shang, *ACS Appl. Mater. Interfaces*, 2013, **5**, 10953–10959.
158 S. Dong, L. Hu, J. Feng, Y. Pi, Q. Li, Y. Li, M. Liu, J. Sun and J. Sun, *RSC Adv.*, 2014, **4**, 64994–65003.